A Szilikátipari Tudományos Egyesület lapja

építőanyag

Journal of Silicate Based and Composite Materials

A TARTALOMBÓL:

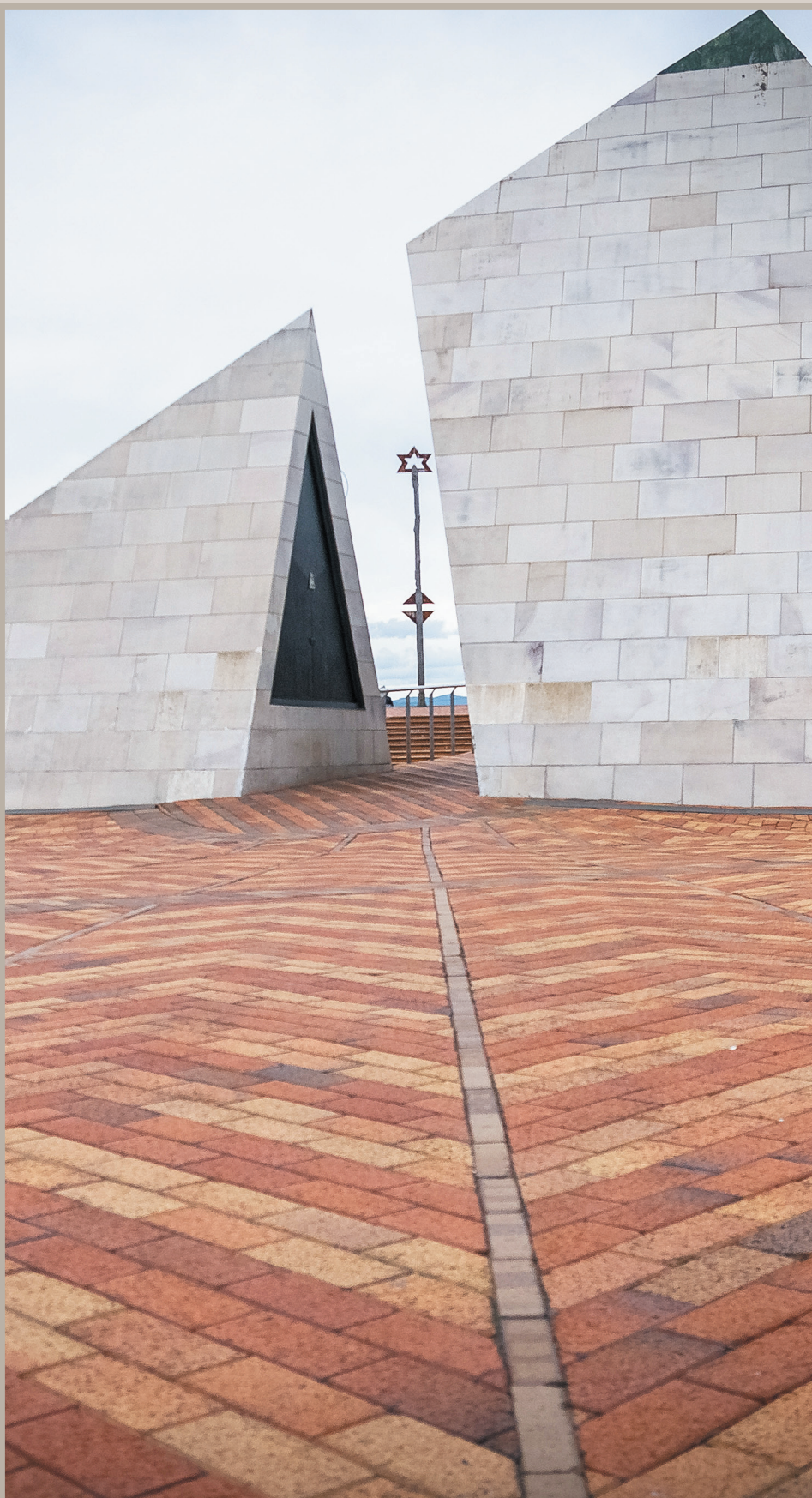

2017/1

nanocem

THE INDUSTRIAL ACADEMIC NANOSCIENCE RESEARCH NETWORK FOR SUSTAINABLE CEMENT AND CONCRETE

Nanocem was founded in 2004, and has grown to a network of 24 academic partners and 10 industry partners. We conduct research at a fundamental level. Yet high levels of industry involvement allow us to focus on solutions that can work in practice and not just in theory.

Our unique model of cooperation between industry and the academic community has led to the identification of common issues, shared knowledge and clear benefits for all those involved. For instance Nanocem has been able to help map the research needs for lower carbon concrete. This guidance helped focus research by companies and third parties. By improving our understanding of cement and concrete, our research leads to innovation that benefits society as a whole.

építőanyag

Journal of Silicate Based and Composite Materials

2017/1

TARTALOM

CONTENT

A finomkerámia-, üveg-, cement-, mész-, beton-, tégla- és cserép-, kő- és kavics-, tűzállóanyag-, szigetelőanyag-iparágak szakmai lapja
Scientific journal of ceramics, glass, cement, concrete, clay products, stone and gravel, insulating and fireproof materials and composites

A folyóiratot referálja · The journal is referred by:
Cambridge Scientific Abstracts
ProQuest

A folyóiratban lektorált cikkek jelennek meg.
All published papers are peer-reviewed.
Kiadó · Publisher: Szilikátipari Tudományos Egyesület (SZTE)
Elnök · President: ASZTALOS István
1034 Budapest, Bécsi út 122–124.
Tel./fax: +36-1/201-9360 ▪ E-mail: epitoanyag@szte.org.hu
Tördelő szerkesztő · Layout editor: NÉMETH Hajnalka

Címlapfotó · Cover photo: KÓSA Luca Kornélia

WWW.EPITOANYAG.ORG.HU
EN.EPITOANYAG.ORG.HU

Online ISSN: 2064-4477
Print ISSN: 0013-970x
INDEX: 2 52 50 ▪ 69 (2017) 1–32

Vol. 69, No. 1

Nest-like $BaO{\cdot}6Fe_2O_3$ microspheres with hierarchical porous structure for drug delivery

S. TORRES-CADENAS ▪ Department of Ceramics Materials, Instituto de Investigación en Metalurgia y Materiales ▪ storres_c@hotmail.com

ALEJANDRO BRAVO-PATIÑO ▪ Centro Multidisciplinario de Estudios en Biotecnología (CMEB) de la FMVZ ▪ abravo@umich.mx

JUAN ZARATE-MEDINA ▪ Department of Ceramics Materials, Instituto de Investigación en Metalurgia y Materiales ▪ jzarate@umich.mx

MARÍA EUGENIA CONTRERAS-GARCÍA ▪ Department of Ceramics Materials, Instituto de Investigación en Metalurgia y Materiales ▪ eucontre@gmail.com

Érkezett: 2016. 11. 19. ▪ Received: 19. 11. 2016. ▪ http://dx.doi.org/10.14382/epitoanyag-jsbcm.2017.1

Abstract

Recent years a surge has been seen in magnetic nanoparticles applications in several areas, particularly in biomedical field. The promising features of the iron oxide based magnetic nanoparticles make them an ideal tool for MRI contrast agents, hyperthermia, and as drug delivery systems (DDS). The present paper describes the design and synthesis of $BaO{\cdot}6Fe_2O_3$ nanostructured meso-macroporous spherical aggregates by sol-gel method via spray drying technique. The obtained spherical aggregates have micrometric size, which let them to be carried by the bloodstream to a specific site where the drug is going to be release. The obtained hierarchical porous structure combined with the interconnected mesoporosity allow the body fluids to be transport through the aggregates; and the macroporosity allows the load of large molecules, like peptides. Furthermore, the structural and morphological characterization of the obtained $BaO{\cdot}6Fe_2O_3$ aggregates were carried out using X-ray diffraction and field emission scanning electron microscopy.

Keywords: Nest-like morphology, hierarchical porous structure, drug delivery, barium hexaferrite.

S. Torres-Cadenas

Biochemical engineer (2009). Master of materials science (2013). Post-graduate student in materials sciences, Department of Advanced Ceramics, IIMM-UMSNH. Work field addresses the design and synthesis of iron oxide-based nanostructured magnetic materials and their physical, chemical and magnetic characterization in order to be applied in biomedical applications such as drug delivery systems.

Alejandro Bravo Patiño

Titular B Profesor and Researcher at Multidisciplinary Research Center in Biotechnology, Universidad Michoacana de San Nicolás de Hidalgo, since 2003. Author and co-author more than 24 publications in indexed international journals. Doctor in sciences with specialization in Biotechnology of Plants. on 1999. At Center for Research and Advanced Studies of I. P. N., Irapuato Unit (CINVESTAV-IRAPUATO). Mexico. Dr. Bravo research interest is in Notch signaling via mammalian embryonic development; interaction of proteins Hairless.

Juan Zarate Medina

lecturer and Researcher, research lines: Synthesis and Processing of Ceramics and Compounds, and Materials Characterization, Work Experience: Titular Researcher C, at Universidad Michoacana de San Nicolás de Hidalgo, UMSNH, since 2002. MS Program Coordinator from 2009 to 2011, PhD Program Coordinator since 2015. Publications: 30+ publications in JCR Journals in the field of Ceramics Materials and Composites. Graduated supervisor: 12 MS and 2 PhD theses in UMSNH.

Dr. María Eugenia Contreras García

Doctor of Sciences since 2000, Titular C Professor and Researcher at the Ceramic Materials Department of the Metallurgy and Materials Research Institute on the Universidad Michoacana de San Nicolás de Hidalgo since 1988 and Level 2 National Researcher since 2001. Specialized on Ceramic Synthesis and Processing Techniques such as ceramic powder processing via sol-gel and chemical techniques, focused on nanostructured ceramics processing and functional ceramics including: structural ceramics, bioceramics, magnetic ceramics, optoelectronic ceramics, catalytic and photocatalytic ceramics, macro-mesoporous ceramics all of them in bulk and in thin films. She is author and co-author of more than 100 international indexed papers, two book chapters and editor in one. She is member of several scientific societies and regional director of the Mexican Academy of Crystallography.

1. Introduction

Recent years a surge has been seen in magnetic nanoparticles applications in several areas such as microelectronics, optoelectronics, physics, chemistry, biology, and materials science, but particularly in biomedical field [1-10]. Several sorts of magnetic nanoparticles have been widely investigated for biomedical applications, among which iron oxide-based magnetic nanoparticles are very promising candidates due to their unique features like biocompatibility, large surface area and superparamagnetic behavior that make them an ideal tool for cell separation, magnetic resonance imaging (MRI) [11-12], cancer treatment by hyperthermia [13-15] drug delivery systems (DDS) [16, 17]. In all these applications it is necessary to maintain the nanostructure of the individual particles in order to preserve the superparamagnetic behavior. This work is focusing on the design and synthesis of meso-macroporous aggregates made from barium hexagonal ferrites ($BaO{\cdot}6Fe_2O_3$) to be applied as DDS. The motivation scheme above mentioned is because of the need to create a DDS that can deliver anticancer drugs at specific sites in a spatiotemporal manner, namely, at particular times and rates. A variety of methods have been reported in the literature on the synthesis of magnetic nanoparticles, such as the chemical co-precipitation, the hydrolysis, the thermal decomposition and the sol-gel technique [18]. We carried out the synthesis of $BaO{\cdot}6Fe_2O_3$ nanostructured meso-macroporous spherical aggregates (hereinafter called $BaO{\cdot}6Fe_2O_3$ aggregates) by the sol-gel method combined with spray drying technique. Sol-gel processing has many advantages, it is an easy and inexpensive method and very pure products are obtained. Size and shape of the particles can be easily controlled. Moreover, the spray drying process has been successfully used to produce porous materials with a spherical shape and a controlled agglomerate size. Great effort is also devoted to characterization, understanding, and improvement of the structural properties of the nanostructured materials. In this work, the design of $BaO{\cdot}6Fe_2O_3$ aggregates has been developed using self-assembly techniques with surfactant Tween-20 as structure directing agent, and polystyrene (PS) templates. This combination of additives is used in order to obtain the hierarchical meso-macroporous structure. A 2f-factorial experimental design was applied to this research in order to obtain the best synthesis and processing conditions that ensure the formation of $BaO{\cdot}6Fe_2O_3$ aggregates that allow the load of specific peptides based anticancer drugs.

2. Materials and experimental procedure

Chemical reagents used for the synthesis of barium hexagonal ferrites were reagent-grade chemicals that were used without further purification: iron (III) nitrate nonahydrate ($Fe(NO_3)3{\cdot}9H_2O$), barium carbonate ($BaCO_3$), ammonium hydroxide (NH_4OH) and Tween-20 ($C_{58}H_{114}O_{26}$) as surfactant. Chemicals used for the synthesis of PS spheres were styrene (monomer, $C_6H_5CH{=}CH_2$) and ammonium persulfate ($(NH_4)_2S_2O_8$). All reagents were provided by Aldrich. Deionized water was used for all the experiments.

2.1 Polystyrene (PS) synthesis

Polystyrene spheres (0.2 microns mean size) were used as pore forming agent (template) in order to obtain macroporous-nanostructured aggregates. The PS spheres were synthetized by our working group. Briefly, the monodisperse PS spheres were synthesized via polymerization. Previously, the styrene monomer was washed with a 1 M sodium hydroxide (NaOH) solution. It was used with a 0.125-wt% ratio for monomer/water. Reaction was carried out under temperature and constant stirring, 60 °C and 300 rpm, respectively. The whole process was taken in 24 hours.

2.2 Design of $BaO{\cdot}6Fe_2O_3$ aggregates.

A 2^f-factorial experimental design was used in order to design the $BaO{\cdot}6Fe_2O_3$ aggregates. The design allowed to evaluate the effect of parameters such as the inlet air pressure (P, Kg/cm^2) and inlet temperature (T, °C) into the spray dryer equipment as well as the template concentration (%) in order to evaluate the pore volume and size of the aggregates obtained in the spray drying process. *Table 1* shows the above factors to evaluate the effect on the pore volume and size of the porous nanostructured aggregates. In the 23-factorial design each factor has two levels: low (-) and high (+). Then a set of eight experiments was performed.

Experiment	Factor						Average diameter (μm)	Pore volume (cm^3/g)	Specific surface area
	A Pressure (P, Kg/cm^2)		B Inlet temperature (T, °C)		C Template concentration (% PS)				
	Low (-) 1.5	High (+) 2	Low (-) 180	High (+) 200	Low (-) 30	High (+) 50			
1	1.5		180		30		1.69	0.0743	14.94
2	1.5		200		30		1.73	0.0639	13.26
3	2.0		180		30		1.71	0.1686	20.42
4	2.0		200		30		1.58	0.0238	16.11
5	1.5		180		50		1.50	0.0463	13.61
6	1.5		200		50		1.64	0.0085	10.86
7	2.0		180		50		1.72	0.1015	7.210
8	2.0		200		50		1.73	0.0143	18.92

Table 1 *Variation levels of the studied parameters and conditions, and the obtained values of the response variables: aggregate average diameter, mesopore volume and specific surface area for the prepared $BaO{\cdot}6Fe_2O_3$ aggregates.*

1. táblázat *A vizsgált paraméterek, a vizsgálati körülmények változékonysága, és a kifejlesztett $BaO{\cdot}6Fe_2O_3$ termék jellemzői: átlagos szemcse átmérő, mezopórus térfogat és fajlagos felület.*

2.3 Synthesis of $BaO{\bullet}6Fe_2O_3$ aggregates

$BaO{\cdot}6Fe_2O_3$ aggregates were synthesized by sol-gel method via spray drying (Mini-Spray Dryer ADL31 Yamato). The former reagents for the synthesis of $BaO{\cdot}6Fe_2O_3$ [$Fe(NO_3)_3{\cdot}9H_2O$ (21 mM) + $BaCO_3$ (1.5 mM)] were dissolved in an aqueous solution with constant stirring for 30 min. At the same time, but separately, Tween-20 (2g/l) was dispersed in deionized water under the same conditions. Both solutions were mixed and kept again under constant stirring for 30 min. The pH value for the obtained suspension was fixed at pH 8, in accordance with a previous study. The mixture was kept under magnetic stirring for 6 h. Next, the solution was mixed homogeneously with PS spheres suspension according to the 23-factorial design and kept under magnetic stirring for 1 hour. The resulting suspension was fed to the spray dryer using the experimental design variables. The obtained aggregates were calcined at 700 °C.

2.4 Characterization

X-ray diffraction (XRD, SIEMENS D-5000) with a Cu Kα radiation (45 KV, 30 mA) was used to determine the crystal structure. Scans were taken from 10° to 80° (2θ) with a constant step width of 0.02°. Scanning electron microscopy was carried out to analyze the microstructural characterization and morphology of the $BaO{\cdot}6Fe_2O_3$. The SEM images were recorded in a field-emission scanning electron microscope JEOL JSM-7600. N2 adsorption/desorption isotherms at 77 K were recorded on a Quantachrome instrument. Prior to analysis, samples (0.14 - 0.38 g) were filled in a tube under N2 atmosphere and then outgassed for 4 h at 100 °C. In addition, the mesopore size distribution was measured by the Barrett-Joyner-Halenda (BJH) technique. The magnetic behavior of the sample calcined at 700°C was carried out at room temperature applying a constant magnetic field of 5000 Oe. The hysteresis loop was recorded in a vibrating sample magnetometer (VSM LDJ 9600). From the hysteresis loop the values for the magnetic saturation (Ms), remnant magnetization (Mr) and coercivity (Hc) were obtained.

3. Results and discussion

Table 1 shows the overall of 8 experiments carried out when used a 23-factorial design and the obtained values for the pore volume and main agglomerates size for all the experiments. Therefore, having an effect about the pore volume and size of the $BaO{\cdot}6Fe_2O_3$ aggregates. Average diameters of the obtained aggregates after the spray drying process and calcined at 700 °C ranged from 1.50 to 1.73 μm. Superparamagnetic iron oxide nanostructured particles ranging from 2.9 nm up to 3.5 μm have been synthesized by various authors. Most of applications are size-dependent. We have chosen to synthetize $BaO{\cdot}6Fe_2O_3$ aggregates of micron size in order to increase the payload on the DDS, assuring the stability of the aggregates during its transport in the bloodstream. Moreover, we have taken in account that the larger aggregate obtained here is capable of being injected even in the capillaries (measuring around 5 to 10 micrometers).

ANOVA								
		Aggregate average diameter			Mesopore Volume			
Factor	Degrees of freedom (DF)	Sum os squares (SS)	Mean square (MS)	Distribution $F(F_0)$-value	Sum of squares (SS)	Mean square (MS)	Distribution $F(F_0)$-value	F_T
A	1	0.49	0.0150	5.74	-0.79	0.063	8.66	
B	1	0.39	0.0095	3.63	-0.50	0.168	3.98	
AB	1	-0.35	0.0076	2.93	0.35	0.023	1.74	
C	1	-0.05	0.0001	0.05	0.46	0.049	2.98	5.32
AC	1	0.15	0.0014	0.53	-0.65	0.008	5.81	
BC	1	0.31	0.0060	2.29	-0.66	0.101	6.02	
ABC	1	0.17	0.0018	0.69	0.59	0.014	4.79	
ERROR	8	0.041	0.0026		0.073	0.0046		
TOTAL	15	0.083			0.227			

Table 2 Analysis of variance of aggregate average diameter and mesopore volume for the prepared $BaO{\bullet}6Fe_2O_3$ aggregates
2. táblázat A kifejlesztett $BaO{\cdot}6Fe_2O_3$ termék átlagos szemcse átmérőjének és mezopórus térfogatának változékonysági vizsgálata.

Statistical analysis of variance (ANOVA) was conducted in order establish which factors aforementioned affected the aggregate size and the mesopore volume of the $BaO{\cdot}6Fe_2O_3$. According to the ANOVA in *Table 2* which analyzes the average aggregate diameter, the only factor that has a significant effect on the aggregate size is pressure. While a minimum effect may be given for the temperature or by the combination of the pressure-temperature and temperature-template. On the other hand, the ANOVA analysis shows that the factor that have a significant effect on the mesopore volume is the pressure alone, in addition to the pressure-template and the temperature-template interaction.

The X-ray diffraction (XRD) pattern of the $BaO{\cdot}6Fe_2O_3$ aggregates is shown in *Fig. 1a.* In a previous study we carried out a thermal analysis in order to determine the optimal temperature to which the pursued hexagonal phase is obtained. The study was performed from 500 up to 1200 °C. Here, we present only XRD pattern of the sample calcined at 700 °C. Scans were made from 10° to 80° (2θ) with a constant step width of 0.02°. The XRD pattern presents three phases, which were identified by using the following Open Database Crystallography, COD cards: the hexaferrite-BaO•6Fe2O3 hexagonal (H), COD card No. 1008841; the monoferrite-$BaFe_2O_4$ orthorhombic (O), COD card No. 4107896; and the magnetite-Fe_2O_3 Hexagonal (F), COD card No. 9015964. The relative intensity of the $BaFe_2O_4$ peaks was found to decrease with increasing the temperature. *Fig. 1b* and *Fig. 1c* shows representative images of scanning electron microscopy (SEM). The images were taken by secondary electrons (SE) at 5.0 KV. It is seen that porous-nanostructured aggregates are made from $BaO{\cdot}6Fe_2O_3$ with a spherical shape. The aggregates were ~1.7 μm average of diameter. A magnification at 15 000 X is presented in the insert of *Fig. 1b* and *Fig. 1c*, where the macroporosity of the nanostructured aggregates of $BaO{\cdot}6Fe_2O_3$ is clearly seen, as a result of the pyrolysis from the PS spheres after being calcined at 700 °C. Moreover, it is seen that a homogeneous-spherical morphology with a 200 nm average macropore size has been formed. Therefore, they fall in the classification of macroporous materials according to the IUPAC. As mentioned earlier, due to the 2^3-factorial design, a set of eight experiments was performed. All samples had a similar structure and morphology, therefore, only the representative images for each of the polystyrene concentrations, 30 and 50-wt%, respectively, are shown. Sample in *Fig. 1b* was synthesized with an inlet temperature at 200 °C and a pressure at 2 Kg/cm^2 corresponding to the parameters on the spray drying, and a concentration of polystyrene spheres of 50-wt%. Sample in *Fig. 1c* was synthesized with an inlet temperature at 180 °C and a pressure at 1.5 Kg/cm^2 corresponding to the parameters on the spray drying, and a concentration of polystyrene spheres of 30-wt%. The main difference between images of *Fig. 1b* and *Fig. 1c* is the pore distribution. A variety of different morphologies have been reported on the literature. For instance, *Kikuo Okuyama* and coworkers [19] have reported completely spherical dense particles, small rough spherical dense particles, highly rough spherical dense particles, hollow particles, doughnut particles, porous particles, encapsulated particles, mixed particles and hairy particles. *Oka Chiemi* and coworkers have reported the synthesis of core-shell composite particles [10], and other morphologies such as nanowires, nanorods, nanoworms, nanotubes and so on have been reported in the literature. We have obtained meso-macroporous $BaO{\cdot}6Fe_2O_3$ nanostructured aggregates with a spherical shape. An advantage of the spherical-shape particles is their practical importance owing to their rheological properties as compared with other morphologies. For example, when on vessels, the flow of the spherical-shape nanoparticles on bloodstream is improved. The morphology of the $BaO{\bullet}6Fe_2O_3$ nanoparticles is elongated fiber-like crosslinked forming a nest-like structure.

Fig. 2 shows the adsorption/desorption isotherms for the samples calcined at 700 °C having template concentrations of 30 and 50 wt%, respectively. Sample in *Fig. 2a* was synthesized with an inlet temperature at 200 °C and a pressure at 2 Kg/cm^2 corresponding to the parameters on the spray drying, and a concentration of polystyrene spheres of 50-wt%. Sample in *Fig. 2b* was synthesized with an inlet temperature at 180 °C and a pressure at 1.5 Kg/cm^2 corresponding to the parameters on the spray drying, and a concentration of polystyrene spheres of 30-wt%. According to BET classification, the isotherms correspond to a typical type II isotherm. The specific surface areas from the $BaO{\cdot}6Fe_2O_3$ aggregates range from 7.21 to 20.42 m^2/g.

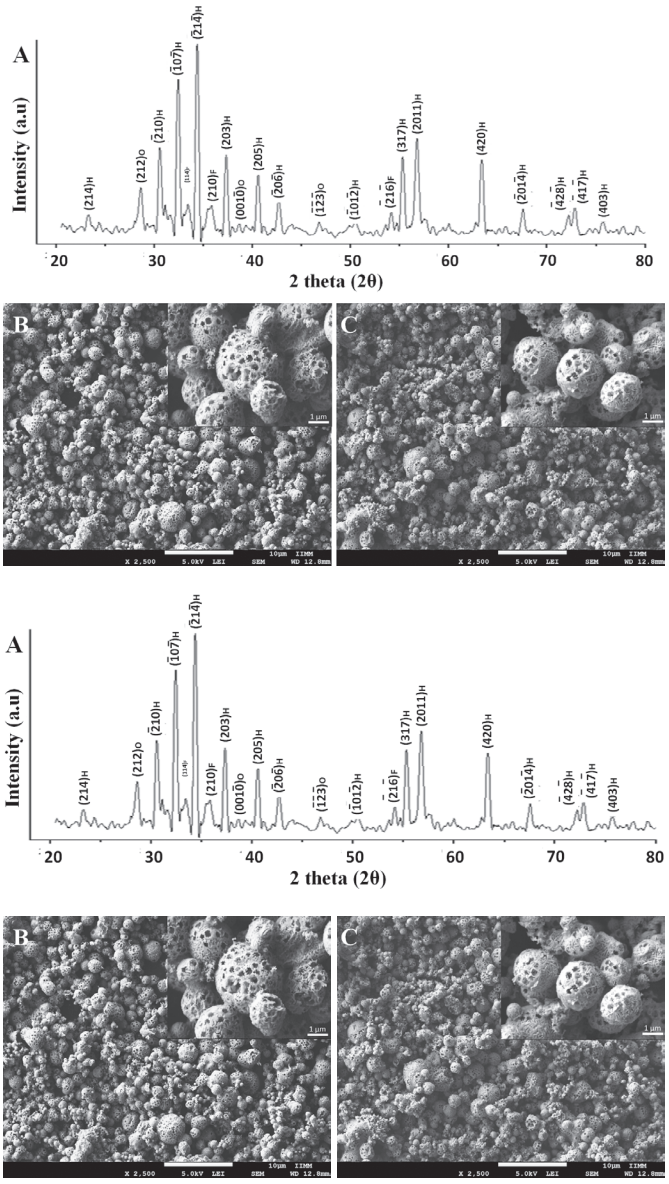

Fig. 1 Structural and morphological characterization of the $BaO{\cdot}6Fe_2O_3$ aggregates calcined at 700 °C showing a) XRD patters having the phases: hexaferrite-$BaO{\cdot}6Fe_2O_3$ hexagonal (H), monoferrite-$BaFe_2O_4$ orthorhombic (O), and the magnetite-Fe_2O_3 hexagonal (F); and SEM images of the $BaO{\cdot}6Fe_2O_3$ with b)50% of PS spheres and c) 30% of PS spheres.

1. ábra A 700 °C hőmérsékleten kalcinált $BaO{\cdot}6Fe_2O_3$ szemcsék szerkezeti és morfológiai jellemzői a) röntgendiffraktogramok a következő fázisokkal: hexagonális hexaferrit-$BaO{\cdot}6Fe_2O_3$ (H), ortorombos monoferrit-$BaFe_2O_4$ (O), és hexagonális magnetit-Fe_2O_3 (F); és pásztázó elektronmikroszkópos felvételek b) 50% PS gömbökkel és c) 30% PS gömbökkel.

Due to the magnetic properties of the iron oxide-based nanostructured systems, in biomedical applications such as drug delivery systems, these materials can benefit from the application of an external magnetic field in order to delivering and targeting a drug to a specific site of action. In order to maintain the magnetic properties that characterize these materials, which are necessary for such applications, the $BaO{\cdot}6Fe_2O_3$ aggregates obtained here were calcined at 700 °C to analyze their magnetic behavior using VSM. *Fig. 3* shows the hysteresis loop from which the values of magnetic saturation (M_s), remnant magnetization (M_r) and coercivity (H_c) were calculated. The obtained values were M_s = 14.24 emu/g, M_r = 5.93 emu/g and H_c = 194.65 Oe, respectively, which represent a low semi-hard magnetic behavior in which the nanoparticulate aggregates can be still safely used for DDS.

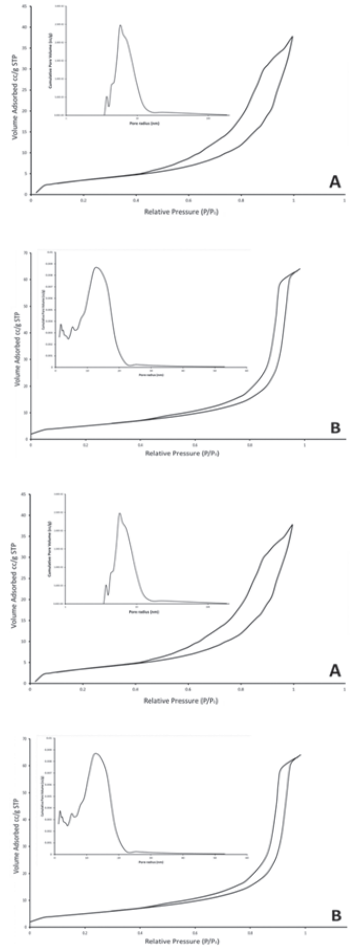

Fig. 2 Adsorption/desorption isotherm plot for the $BaO{\cdot}6Fe_2O_3$ aggregates, relative pressure (P/P_0) as a function of N2 volume adsorbed (cm^3/g) at STP.

2. ábra A kifejlesztett $BaO{\cdot}6Fe_2O_3$ szemcsék adszorpciós/deszorpciós izotermái.

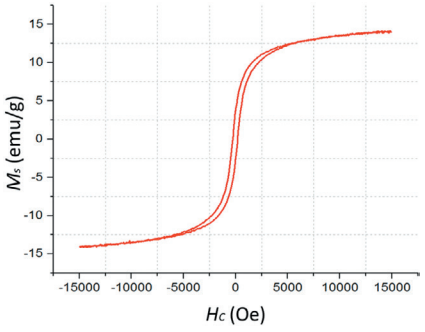

Fig. 3 Hysteresis loop from the $BaO{\cdot}6Fe_2O_3$ aggregates calcined at 700 °C.

3. ábra Hiszterézis hurok illusztrációja 700 °C hőmérsékleten kalcinált $BaO{\cdot}6Fe_2O_3$ szemcsékhez.

4. Conclusions

Design and synthesis of $BaO{\cdot}6Fe_2O_3$ nanostructured meso-macroporous spherical aggregates was possible through a 2^3-factorial design by using a sol-gel method via spray drying. A number of three factors were evaluated including the pressure and the inlet temperature corresponding to the spray drying process as

well as the template concentration on the wet chemical synthesis. Evaluation through an analysis of variance (ANOVA) showed that not only the individual factors including the PS concentration and the pressure corresponding to the spray drying process affected the morphology and the size of the meso-macroporous $BaO{\cdot}6Fe_2O_3$ aggregates, but the interaction between the pressure and the inlet temperature as well. Meso-macroporous-$BaO{\cdot}6Fe_2O_3$ nanostructured spherical-shape aggregates with a diameter of 1.7 μm were obtained. The spherical-shape was confirmed by scanning electron microscopy. Characterization of meso-macroporous $BaO{\cdot}6Fe_2O_3$ nanostructured systems shows that the formulation used here, as well as parameters involved in the sol-gel method via spray drying can be used as a good approach in order to synthetize effective magnetic nanoparticles conforming micrometric spherical aggregates with meso-macroporous structure for the load of large molecules like peptides to be used as drug delivery systems.

References

[1] Ma, M. – Zhang, Y. – Yu, W. – Shen, H. – Zhang, H. – Gu, N. (2003): Preparation and characterization of magnetite nanoparticles coated by amino silane. *Colloids and Surfaces A: Physicochem. Eng. Aspects.* Vol. 212, pp. 219-226, http://dx.doi.org/10.1016/S0927-7757(02)00305-9

[2] Gupta, A. K. – Gupta, M. (2005): Synthesis and surface engineering of iron oxide nanoparticles for biomedical applications. *Biomaterials.* Vol. 26, No. 18, June 2005, pp. 3995–4021, http://dx.doi.org/10.1016/j.biomaterials.2004.10.012

[3] Ichiyanagi, Y. – Kubota, M. – Moritake, S. – Kanazawa, Y. – Yamada, T. – Uehashi, T. (2007): Magnetic properties of Mg-ferrite nanoparticles. *Journal of Magnetism and Magnetic Materials.* Vol. 310, No. 2, March 2007, pp. 2378–2380, http://dx.doi.org/10.1016/j.jmmm.2006.10.737

[4] Chertok, B. – Moffat, BA. – David, A.E. – Yu F. – Bergemann, C. – Ross, B.D. – Yang, V.C. (2008): Iron oxide nanoparticles as a drug delivery vehicle for MRI monitored magnetic targeting of brain tumors. *Biomaterials.* Vol. 29, No. 4, February 2008, pp. 487–496, http://dx.doi.org/10.1016/j.biomaterials.2007.08.050

[5] Shubayev V. I. – Pisanic II T. R. – Jin S. (2009): Magnetic nanoparticles for theragnostics. *Advanced Drug Delivery Reviews.* Vol. 61, No. 6, June 2009, pp 467–477, http://dx.doi.org/10.1016/j.addr.2009.03.007

[6] Chomoucka, J. – Drbohlavova, J. – Huska D. – Adam, V. – Kizek, R. – Hubalek, J. (2010): Magnetic nanoparticles and targeted drug delivering. *Pharmacological Research.* Vol. 62, No. 2, August 2010, pp. 144–149, http://dx.doi.org/10.1016/j.phrs.2010.01.014

[7] Tung, W. L. – Hu, S. H. – Liu, D. M. (2011): Synthesis of nanocarriers with remote magnetic drug release control and enhanced drug delivery for intracellular targeting of cancer cells. *Acta Biomaterialia.* Vol. 7, No. 7, July 2011, pp. 2873–2882, http://dx.doi.org/10.1016/j.actbio.2011.03.021

[8] Yelenich, O. V. – Solopan, S. O. – Kolodiazhnyi, T. V. – Dzyublyuk, V. V. – Tovstolytkin, A. I. – Belous, A. G. (2013): Superparamagnetic behavior and AC-losses in $NiFe_2O_4$ nanoparticles. *Solid State Sciences.* Vol. 20, June 2013, pp. 115–119, http://dx.doi.org/10.1016/j.solidstatesciences.2013.03.013

[9] An, G. H. – Hwang, T. Y. – Kim, J. – Kim, J. – Kang, N. – Kim, S. – Choi, Y. M. – Choa, Y. H. (2014): Barium hexaferrite nanoparticles with high magnetic properties by salt-assisted ultrasonic spray pyrolysis. *Journal of Alloys and Compounds.* Vol. 583, January 2014, pp. 145–150, http://dx.doi.org/10.1016/j.jallcom.2013.08.105

[10] Oka, C. – Ushimaru, K. – Horiishi, N. – Tsuge, T. – Kitamoto, Y. (2015): Core-shell composite particles composed of biodegradable polymer particles and magnetic iron oxide nanoparticles for targeted drug delivery. *Journal of Magnetism and Magnetic Materials.* Vol. 381, May 2015, pp. 278–284, http://dx.doi.org/10.1016/j.jmmm.2015.01.005

[11] Lam, T. – Pouliot, P. – Avti, P. K. – Lesage, F. – Kakkar, A. K. (2013): Superparamagnetic iron oxide based nanoprobes for imaging and theranostics. *Advances in Colloid and Interface Science.* Vol. 199–200, November 2013, pp. 95–113, http://dx.doi.org/10.1016/j.cis.2013.06.007

[12] Chen, Y. – Ai, K. – Liu, J. – Sun, G. – Yin, Q. – Lu, L. (2015): Multifunctional envelope-type mesoporous silica nanoparticles for pH-responsive drug delivery and magnetic resonance imaging. *Biomaterials.* Vol. 60, August 2015, pp. 111–120, http://dx.doi.org/10.1016/j.biomaterials.2015.05.003

[13] Cohen, Y. – Shoushan, S. Y. (2013): Magnetic nanoparticles-based diagnostics and theranostics. *Current Opinion in Biotechnology.* Vol. 24, No. 4, August 2013, pp. 672–681, http://dx.doi.org/10.1016/j.copbio.2013.01.006

[14] Tabatabaei, S. N. – Girouard, H. – Carret, A. S. – Martel, S. (2015): Remote control of the permeability of the blood-brain barrier by magnetic heating of nanoparticles: A proof of concept for brain drug delivery. *Journal of Controlled Release.* Vol. 206, May 2015, pp. 49–57, http://dx.doi.org/10.1016/j.jconrel.2015.02.027

[15] Arcos, D. – Vallet-Regí, M. (2013): Bioceramics for drug delivery. *Acta Materialia.* Vol. 61, No. 3, February 2013, pp. 890–911, http://dx.doi.org/10.1016/j.actamat.2012.10.039

[16] Hałupka-Bryl, M. – Bednarowicz, M. – Dobosz, B. – Krzyminiewski, R. – Zalewski, T. – Wereszczyńska, B. – Nowaczyk, G. – Jarek, M. – Nagasaki, Y. (2015): Dooxorubicin loaded PEG-b-poly(4-vinylbenzylphosphonate) coated magnetic iron oxide nanoparticles for target drug delivery. *Journal of Magnetism and Magnetic Materials.* Vol. 384, June 2015, pp. 320-327, http://dx.doi.org/10.1016/j.jmmm.2015.02.078

[17] Yadavalli, T. – Ramasamy, S. – Chandrasekaran, G. – Michael, I. – Therese, H. A. – Chennakesavulu, R. (2015): Dual responsive PNIPAM-chitosan targeted magnetic nanopolymers for targeted drug delivery. *Journal of Magnetism and Magnetic Materials.* Vol. 380, pp. 315-320, http://dx.doi.org/10.1016/j.jmmm.2014.09.035

[18] Komarneni, S. – Hu, W. – Noah, D. Y. – Orden, A. V. – Feng, S. – Wei, C. – Pang, H. – Gao, F. – Lu, Q. – Katsuki, H. (2012): Magnetite syntheses from room temperature to 150 °C with and without microwaves. *Ceramics International.* Vol. 38, No. 3, April 2012, pp. 2563-2568, http://dx.doi.org/10.1016/j.ceramint.2011.11.027

[19] Ratna Balgisa, R. – Iskandara, F. – Ogic, T. – Purwantod, A. – Okuyama, K. (2011): Synthesis of uniformly porous NiO/ZrO_2 particles. *Materials Research Bulletin.* Vol. 46, No. 5, May 2011, pp. 708–715, http://dx.doi.org/10.1016/j.materresbull.2011.01.019

Ref.:

Torres-Cadenas, S. – **Bravo-Patiño**, A. – **Zarate-Medina**, J. – **Contreras-García**, M. E.: *Nest-like $BaO{\cdot}6Fe_2O_3$ microspheres with hierarchical porous structure for drug delivery*
Építőanyag – Journal of Silicate Based and Composite Materials, Vol. 69, No. 1 (2017), 2–6. p.
http://dx.doi.org/10.14382/epitoanyag-jsbcm.2017.1

Hierarchikus pórusszerkezetű $BaO{\cdot}6Fe_2O_3$ mikrogömb szemcsék fejlesztése gyógyhatóanyag közvetítéséhez

A mágneses tulajdonságú nano-részecskék alkalmazási lehetőségeinek kutatása fokozódik napjainkban, különösen a gyógyászati területen. A vasoxid bázisú mágnesezhető nano-részecskék ideálisak MRI kontrasztanyagként vagy gyógyhatóanyag továbbítására. A cikk bemutatja a hierarchikus pórusszerkezetű $BaO{\cdot}6Fe_2O_3$ mikrogömb szemcsék fejlesztését szol-gél módszerrel. A kifejlesztett, gömb alakú aggregátum mikro-méretű szemek halmaza, amely a véráramban könnyen mozgatható és ezáltal a gyógyhatóanyag meghatározott helyre továbbítható bennük. A hierarchikus pórusszerkezet az összekapcsolódó mezo-pórusok révén lehetővé teszi nagyméretű molekulák pl. peptidek szállítását és lehetőséget biztosít a testfolyadékok általi kimosásukra. A kifejlesztett $BaO{\cdot}6Fe_2O_3$ nano-részecskék jellemzőit és hatékonyságát röntgendiffrakciós és pásztázó elektronmikroszkópos vizsgálatok eredményeivel illusztrálják a szerzők.

Kulcsszavak: fészekszerű morfológia, hierarchikus pórus-szerkezet, gyógyhatóanyag továbbítás, barium-hexaferrit.

Környezetbarát Cement- és Betonipari Technológiák

MUCSI GÁBOR ▪ GÁVEL VIKTÓRIA

Szakmai nap a Miskolci Egyetemen

2017. május 24-én került megrendezésre a „Környezetbarát Cement- és Betonipari Technológiák" c. szakmai nap a Szilikátipari Tudományos Egyesület, Cement Szakosztálya, Beton Szakosztálya, az MTA Földtudományok Osztály, Bányászati Tudományos Bizottság, Bányászati, Geotechnikai és Nyersanyagelőkészítési Albizottsága, az MTA MAB Nyersanyagelőkészítési és Környezeti Eljárástechnikai Munkabizottsága, valamint a Miskolci Egyetem, Műszaki Földtudományi Kar, Nyersanyagelőkészítési és Környezeti Eljárástechnikai Intézete, továbbá az Országos Magyar Bányászati és Kohászati Egyesület Miskolci Egyetemi Szakosztálya szervezésében. A rendezvénynek a Miskolci Egyetem adott otthont, melyen három egyetem és egy kutatási-fejlesztési cég szakemberei tartottak előadásokat.

A szakmai ülés apropóját az adta, hogy világviszonylatban jelentős mennyiségű ipari melléktermék, hulladék keletkezik évente, amely hasznosítása a megfelelő technológiák alkalmazásával, továbbfejlesztésével megoldható, továbbá környezetbarát anyagok fejlesztésére ad lehetőséget a CO_2 kibocsájtás és energiaigény csökkentése, továbbá a fenntartható nyersanyag-gazdálkodás révén.

Az elhangzott előadások is ezt a témakört célozták meg. A szakmai nap programja az alábbi volt:

Megnyitó, Köszöntő
Mucsi Gábor egyetemi docens, Miskolci Egyetem, SZTE Cement Szakosztály elnöke

Energiatakarékos beton
Gável Viktória tanúsítási irodavezető, Cemkut Kft.

Alkáli aktivált cementek előállítása kristályos kohókőből
Balczár Ida Anna egyetemi tanársegéd, Korim Tamás egyetemi docens, Pannon Egyetem

Környezetbarát cementek alkalmazása
George Nehme Salem egyetemi docens, Budapesti Műszaki és Gazdaságtudományi Egyetem

Geopolimer habok fejlesztése ipari melléktermékekből
Szabó Roland PhD hallgató, Mucsi Gábor egyetemi docens, Miskolci Egyetem

„Innovatív Finomőrlési-Szemcsetervezési Technológiák Laboratórium Fejlesztése A Miskolci Egyetem Fenntartható Természeti Erőforrás Gazdálkodás Kiválósági Központban" című GINOP 2.3.3. projekt bemutatása
Rácz Ádám adjunktus, Miskolci Egyetem

A tudományos előadásokat, egy a Miskolci Egyetemen nemrég indult projekt ismertetője követte, amely keretében beszerzésre kerülő eszközök (kamerás szemcseméret-elemző, multifunkciós por reométer, nagy energiasűrűségű bolygómalom, izotermikus kaloriméter, asztali pásztázó elektron-mikroszkóp, BET fajlagos felület mérő, végeselemes módszeren alapuló, szemcsés anyagok viselkedését modellező szoftver) nagymértékben hozzájárulnak majd a szakterületen jelentkező K+F+I ipari igények kiszolgálására a többi kutatóműhellyel szorosan együttműködve. A tanácskozást egy büféebéd, majd egy laboratóriumi látogatás követte, amelyen a résztvevők megtekinthették a Műszaki Földtudományi Karhoz tartozó jól felszerelt laboratóriumokat. A rendezvényen elhangzott információk rávilágítottak arra, hogy milyen nagy szükség van a tématerületen dolgozó mérnökökre (cementgyárak, betonüzemek, hulladékelőkészítőművek) nemcsak hazánkban, hanem világszerte.

A szakmai nap jó lehetőséget biztosított a területen működő cégek (cementgyárak, betonüzemek, minősítő szervezetek) és a kutatás – fejlesztés szakembereinek az eszmecserére, mivel közel 50 fő jelent meg.

A Szervezők bíznak a kutatóhelyek és ipari cégek által megkezdett együttműködések folytatásában mind a kutatás-fejlesztés-innováció, mind pedig a felsőfokú oktatás vonatkozásában, valamint a szakmai nap rendszeres megrendezésével hagyományt kívánnak teremteni.

Titania-Ceria surfactant assisted sol-gel synthesis and characterization

A. TORRES-ROMERO ▪ IIMM UMSNH ▪ abigailtorresromero2014@gmail.com
M. CAJERO-JUÁREZ ▪ IIAF UMSNH ▪ eucontre@gmail.com
M. E. CONTRERAS-GARCÍA ▪ IIMM UMSNH ▪ cajeromarco@hotmail.com

Érkezett: 2016. 11. 19. ▪ Received: 19. 11. 2016. ▪ http://dx.doi.org/10.14382/epitoanyag-jsbcm.2017.2

Abstract

The nanoparticles of titanium dioxide are important in a wide range of applications such as catalysis, environmental remediation and solar energy conversion. While cerium oxide is rare-earth oxide material used in the fields of photoluminescence, photosensitive material to UV radiation. Furthermore, research on the synthesis of nanoparticles of titanium dioxide has given rise to different methods such as sol-gel, in solid states, hydrothermal processes, among others. The process of solid state synthesis is most often used for the technical production of ceramic materials, while the sol-gel has gained much popularity in recent decades. Between these methods, microemulsion of reverse micelles technique, is one of the most versatile allowing control of particle properties such as size distribution, morphology and surface area. In this work, titania-ceria nanoparticles in anatase phase were synthesized by sol-gel method assisted by microemulsion reverse micelle using titanium butoxide and cerium nitrate hexahydrate as the precursors. The sample was thermally treated at 600 °C at a rate of 3 °C min-1. The residence time of the sample at this temperature was 2 hrs. TEM and XRD analysis were used to characterize the samples obtained. According to the results, the obtained nanoparticles present spherical morphology and have a size distribution of 5 nm for CeO_2, 9.5 for TiO_2 and 14, 17 and 20 nm for the doped TiO_2 with 5, 10 and 15% CeO_2, respectively. The results indicate that the CeO_2 was incorporated into the network of titania.

Keywords: nanoparticles, titania, ceria, microemulsion, sol-gel.

A. Torres-Romero
Master of sciences since 2015, post-graduate student in Ceramic Biomaterials, Department of Advanced Ceramics, Metallurgy and Materials Research Institute on the Universidad Michoacana de San Nicolás de Hidalgo. She is specialist in sciences of biofunctionalization and synthesis of ceramic materials. Her teaching experience includes: introduction to bioassays, technical capacitation and analytical methods design.

M. E. Contreras-García
Doctor of Sciences since 2000, Titular C Professor and Researcher at the Ceramic Materials Department of the Metallurgy and Materials Research Institute on the Universidad Michoacana de San Nicolás de Hidalgo since 1988 and Level 2 National Researcher since 2001. Specialized on Ceramic Synthesis and Processing Techniques such as ceramic powder processing via sol-gel and chemical techniques, focused on nanostructured ceramics processing and functional ceramics including: structural ceramics, bioceramics, magnetic ceramics, optoelectronic ceramics, catalytic and photocatalytic ceramics, macro-mesoporous ceramics all of them in bulk and in thin films. She is author and co-author of more than 100 international indexed papers, two book chapters and editor in one. She is member of several scientific societies and regional director of the Mexican Academy of Crystallography.

M. Cajero-Juárez
Doctor in Genetic and Molecular Biology, Titular C Professor and Researcher at the Animal Biotechnology Laboratory of the IIAF on the Universidad Michoacana de San Nicolás de Hidalgo and National Researcher. Specialized on animal genome manipulation, gene expression on cells and synthetic biology for gene and protein design.

1. Introduction

Nanomaterials based on metal oxides exhibit remarkable physical and chemical properties that enable the development of novel nanodevices that can be used in different physical, biological, biomedical and pharmaceutical applications [1-7]. The surface of these nanostructures is crucial for these applications. These nanostructures excel in catalytic applications because of the presence of surface defects that act as active sites for adsorption of reactive molecules [6]. These defects present in the nanoparticles, especially cerium dioxide and titanium, increase the active surface area that favors the union of a large variety of ligands on its surface [8]. Although so far the use of nanoparticles of titania and ceria in the biomedical and therapeutic area has been carried out separately and not mixed [3-7], it is possible to hardness the power possessed by lanthanide ions with electronic configuration 4f, as cerium, which when entering the network of the titania acts as an electronic trap [9-10], which could increase the number of molecules captured on its surface, which will be extremely useful for increasing the binding of drugs in nanoparticles of titania and improve its efficiency as a nanocarrier.

Furthermore, research on the synthesis of these nanomaterials has given rise to different methods such as sol-gel, solid, chemical vapor deposition, hydrothermal processes, among others. The process of solid state synthesis is most often used for the production of technical ceramic materials, while the sol-gel has gained much popularity in recent decades [3]. These methods microemulsion technique reverse micelles is one of the most versatile allowing control of particle properties such as size distribution, morphology and surface area [5]. The reverse micelles are used as a micro-heterogeneous medium for generating nanoparticles, where microcavities surfactant provide a similar effect to a cage which influences the particle nucleation, growth and agglomeration. The scale of these nanoreactors size is in the range 2 to 10 nm. This is a dynamic system on a micellar level. Micelles collide with each other and quickly share their content, which is essential for carrying out chemical reactions [11].

In this work a combined method for synthesis of TiO_2 nanoparticles doped CeO_2, for use as drug delivery systems described. Using Tween-20 as surfactant, as cosurfactant methanol, toluene as continuous phase and titanium butoxide and cerium nitrate as precursors.

2. Materials and methods

All reagents used in this study were of analytical grade, $Ti(OC_4H_9)_4$ (98%, Aldrich), $Ce(NO_3)_3{\cdot}6H_2O$ (99.8%, Merck), C_7H_8 (99.5%, Merck), CH_3OH (99.8%, Merck), $C_{58}H_{114}O_{26}$ (Merck) and deionized water (Merck).

2.1 Nanoparticles synthesis

TiO_2, CeO_2 and TiO_2-CeO_2 nanoparticles were synthetized by sol-gel method assisted by a surfactant. The precursor $Ce(NO_3)_3{\cdot}6H_2O$ was dissolved in 2 mL of deionized water (0, 5, 10 and 15 mol%), then slowly added to an organic phase

Tween-20/methanol/toluene in a v/v ratio of 6/1/10 mL and was at a temperature of 60 °C for 10 min, then added drop by drop the titanium butoxide (in the following proportions: 100, 95, 90 and 85 mol%) while preserving the conditions of temperature and agitation for 40 min. The resulting suspension remained standing at room temperature protected from light for 12 hrs. The synthesis of nanoparticles becomes evident that is possible to observe the separation of the microemulsion into two layers. The upper layer is recovered and subjected to drying at 100 °C in an oven for 24 hrs, the resulting powder sample was heat treated at 600 °C at a rate of 3 °C / min[1]. The residence time of the sample at this temperature was 2 hrs.

2.2 Characterization

The structural and chemical characterization of the nanoparticles was made from powder samples obtained in the synthesis. The samples were prepared in the form of dilutions of varied concentration (according to the analysis technique), and powders obtained from the heat treatment. The characterization techniques that were used were: X-ray diffraction, XRD and conventional and high resolution transmission electron microscopy, TEM and HRTEM.

3. Results and discussion

3.1 Nanoparticles synthesis

The synthesis process from the hydrolysis reaction of titanium butoxide and the insertion of cerium nitrate into the micelles formed by Tween-20 and methanol under acidic conditions (pH 5) was manifested by the separation of the microemulsion in two layers upon completion of 40 minutes of reaction. The upper layer consists of the organic phase containing the non-agglomerated nanoparticles and the lower layer is treated with the inorganic phase [12].

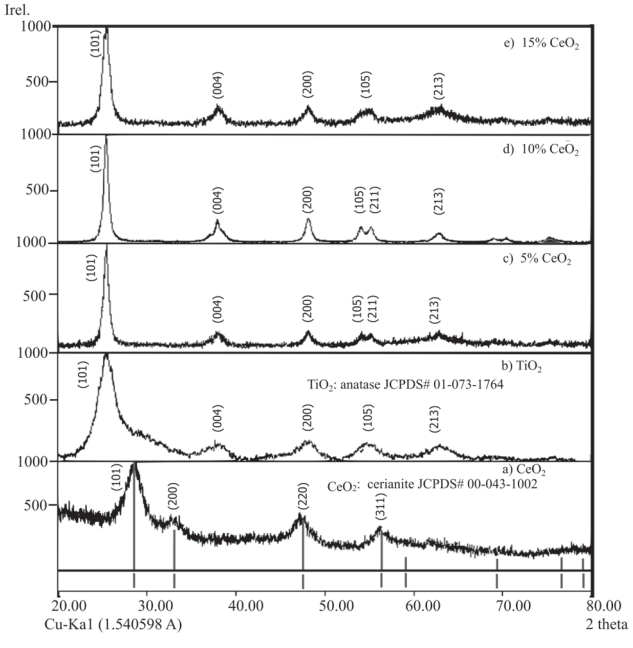

Fig. 1 Diffraction patterns obtained from CeO_2 powders (a), TiO_2 (b) doped 5% (c), 10% (d) and 15% CeO_2 (e).
1. ábra Röntgendiffraktogramok: (a) CeO_2, (b) TiO_2, (c) TiO_2 + 5% CeO_2, (d) TiO_2 + 10% CeO_2, (e) TiO_2 + 15% CeO_2

In *Fig. 1*, the diffraction patterns of the single TiO_2 (a) and doped with (b) 5%, (c) 10% and (d) 15% CeO_2 powders are shown. In the four diffraction patterns only the reflections corresponding to the anatase phase of titanium dioxide (JCPDS # 01-071-1166) could be identified; while in the three doped titania patterns, the Bragg peaks corresponding to the doping species, CeO_2, were not observed, suggesting the incorporation of CeO_2 in the TiO_2 network. It can also be observed in these three diffraction patterns that, as the CeO_2 percentage increases.

The average crystallite size (TC) for the four systems studied was determined by the Debye-Scherrer formula, the results of the measurements are shown in *Fig. 2*. When comparing these results with the simple nanoparticles obtained by this same method, it can be seen that when doping the TiO_2 nanoparticles with CeO_2, the average grain size increases, however as the percentage of dopant increases the size of crystallite decreases, this may be due to the segregation of the dopant cations at the grain boundary may prevent the growth of nanocrystallite in the nanoparticles [2, 13-14]. Another possible cause is that the Ce^+ ion absorbed in the titania network decreases the free surface energy of the particles, which inhibits the process of aggregation of the nanoparticles [2, 15].

The microstructural effect of spreading in the peaks is the presence of residual stresses in the material due to the inclusion of the cerium atoms in the titania network, causing a deformation of its crystalline planes. In this particular case the effect is presented at the microscopic level, causing a widening of the diffraction profile with respect to the original position of the standard pattern diffraction peaks [9-10]. The evaluation of the microtensions was carried out from the displacement of the crystalline plane (101) of the titania, because they suffer a variation in the interplanar distances caused by the internal residual forces, the results of the estimations are shown in the *Fig. 2*.

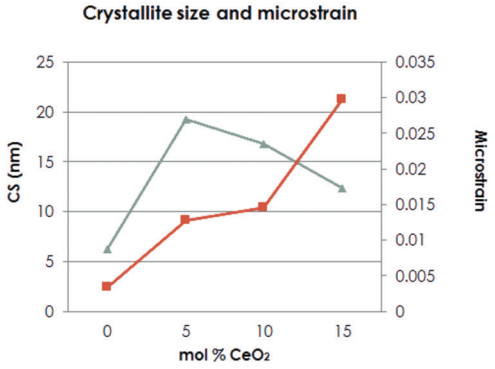

Fig. 2 Crystallite size measurements and microtensile diffraction patterns simple and TiO_2, doped 5%, 10% and 15% CeO_2.
2. ábra Krisztallit méret és mikrodeformáció: CeO_2, TiO_2 + 5% CeO_2, TiO_2 + 10% CeO_2, TiO_2 + 15% CeO_2

From the measurements of the crystallite size and microtension in the diffraction patterns of the powders of simple titania and ceria doped, represented in *Fig. 2*, it is possible to affirm that for the case of simple TiO_2 the increase in the maximum width a half peak (FWHM), is only provoked by the decrease in crystallite size; whereas for the powders of doped titania, it is mainly due to the microdeformations caused in their crystalline planes when the ceria atoms are incorporated and the decrease

of the crystallite size is possibly the result of an increase in the percentage of dopant incorporated in their network. This effect is more noticeable in the system doped with 15% of ceria because when using higher percentages of CeO_2, the greater the tension provoked in the network that of the titania.

The crystallographic data of the phase identified in the pattern of *Fig. 1a* (TiO_2: JCPDS # 01-073-1764) were used as crystalline model from the obtained diffraction patterns. In *Fig. 3*, it is seen that as the dopant percentage increases, CeO_2, the Ti factor occupying factor in the unit cell decreases, this suggests that the cerium atoms are incorporated in the titania network by displacing these Atoms.

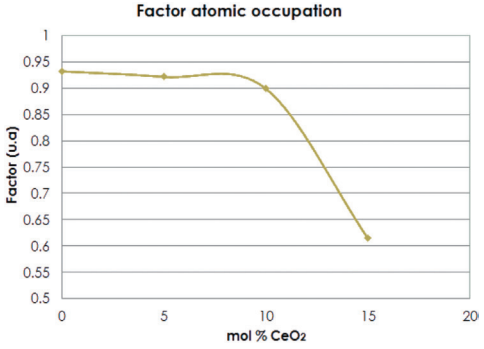

Fig. 3 Factor atomic occupation of simple and TiO_2, doped 5%, 10% and 15% CeO_2.
3. ábra Atom illeszkedési tényező: CeO_2, TiO_2 + 5% CeO_2, TiO_2 + 10% CeO_2, TiO_2 + 15% CeO_2

Fig. 4 shows a high-resolution image, accompanied by its corresponding Fast Fourier Transform (FFT), taken from the TiO_2 sample. The selected nanoparticle has a size which is about 8.5 nm, in which an interplanar distance of about 0.343 nm, corresponding to the plane (101) of the tetragonal cubic structure of TiO_2, could be measured. Likewise, in their respective FFT, the periodic arrangement of the points makes evident the crystalline character of the particle.

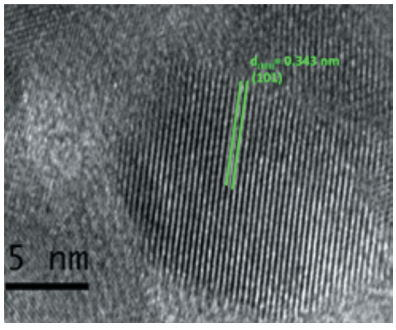

Fig. 4 High resolution micrograph of a nanoparticle showing an interplanar distance of 0.343 nm.
4. ábra Nano-részecske nagy felbontású mikroszkópos felvétele: 0,343 nm síktávolság figyelhető meg

Fig. 5a corresponds to a high resolution image of the doped sample, where spheroidal nanoparticles with a diameter of 20 nm are observed, which is in agreement with the crystallite size estimated from the main intensity in the pattern i.e. the doping at low percentages of CeO_2 increases the size of crystallite and thus the particle diameter; it can be thought that the main reason for this growth is because the radius of the cerium atom is more large that the Ti^+ and to enter in low percentages causes that the nanoparticles increase their size. While in *Fig. 5b*, a nanoparticle with an approximate size of 22 nm is observed, in which an interplanar distance of approximately 2.48 Å, corresponding to the plane (101) of the tetragonal cubic structure of TiO_2. This reinforces the observations in the diffraction patterns, which suggests the incorporation of CeO_2 in the TiO_2 network [16-18].

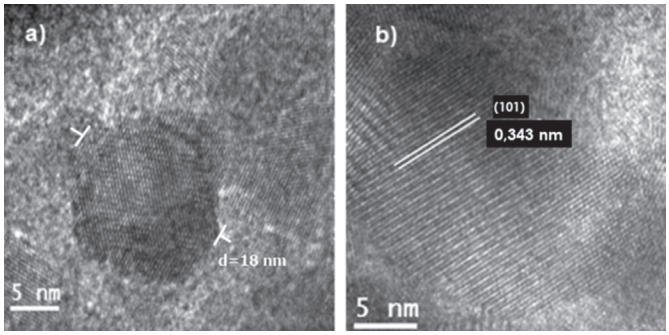

Fig. 5 HRTEM micrographs. One observed nanoparticles of 18 nm (a), a nanoparticle exhibiting an interplanar distance of 0.343 nm (b).
5. ábra Nagy felbontású mikroszkópos felvételek (a) 18 nm méretű nano-részecske, (b) nano-részecske 0,343 nm síktávolsággal.

Fig. 6a and *6b* shows clear field micrographs at a magnification of 690,000×, taken in different areas of the doped titania sample with 15% CeO_2, where it is observed that the nanoparticles have average diameters of 14 nm. As can be seen in the micrographs, the particle size decreases with increasing dopant percentage, suggesting that the cerium ion upon incorporation into the titania network slows the growth of the nanoparticles.

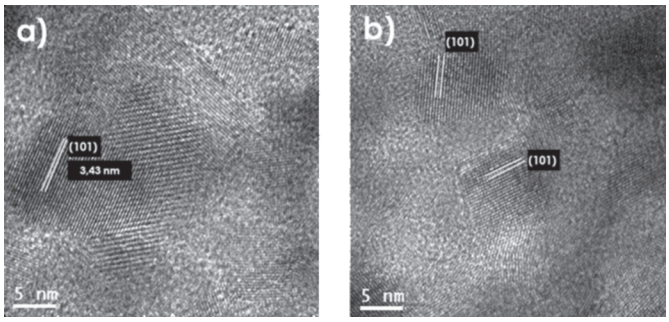

Fig. 6 Brightfield TEM micrographs with a magnification of 690,000×, in which a group of spheroidal TiO_2 nanoparticles doped 15% CeO_2 is observed.
6. ábra Brightfield TEM felvételek 690.000× nagyítással; gömbszerű nano-részecskék figyelhetők meg

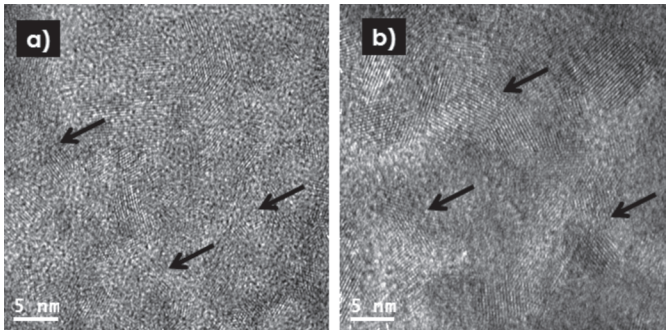

Fig. 7 Light field micrographs with a magnification of 99,000×, obtained by TEM.
7. ábra Light field TEM felvételek 99.000× nagyítással

Fig. 7a and *7b* correspond to clear-field micrographs taken from a CeO_2 sample, in which spheroidal nanoparticles with an average size of 5 nm (indicated by arrows) are observed. These

results indicate that using the proposed methodology can be obtained CeO_2 nanoparticle, and suggesting that during the joint process of synthesis and doping both types of nanoparticles, however, because the CeO_2 nuclei are smaller, due to the low concentration of reagent, gives a secondary nucleation, where the nanoparticles of TiO_2 are formed [12, 19].

4. Conclusions

The conditions for the synthesis of nanoparticles of TiO_2 doped with ceria were established by the inverse micelles method, emphasizing the surfactant handling and the formation of suspensions in which the material is synthesized.

By the microemulsion method of reverse micelles, nanoparticles of anatase phase titania and titania doped with ceria of spheroidal shape were obtained with an average diameter of 9.5, 14 and 20 nm, respectively. This suggests that in the interior of the micelles there is a greater availability of water to carry out the hydrolysis and dopant insertion reaction in the TiO_2 nanoparticles, which favors the nucleation stage, so it is probable that Increase the number of nuclei produced thereby forming smaller particles.

5. Acknowledgments

This research was funded by CIC UMSNH (Universidad Michoacana de San Nicolás de Hidalgo, México) and CONACYT (Consejo Nacional de Ciencia y Tecnología, México), A. Torres-Romero, received a doctoral grant from CONACYT.

References

[1] Oskam, G. – Nellore, A. – Penn, R. L. – Searson, P. C. (2003): The growth kinetics of TiO_2 nanoparticles from titanium (IV) alkoxide at high water/titanium ratio. *The Journal of Physical Chemistry B*, 107(8), 1734-1738. https://doi.org/10.1021/jp021237f

[2] Xu, J. – Ao, Y. – Fu, D. (2009): A novel Ce, C-codoped TiO_2 nanoparticles and its photocatalytic activity under visible light. *Applied Surface Science*, 256(3), 884-888. https://doi.org/10.1016/j.apsusc.2009.08.079

[3] Sitthisang, Onthikan – Komarneni, Sridhar – Tantirungrotechai, Jonggol – Dong Noh, Young – Li, Huihui – Yin, Shu – Sato, Tsugio – Katsuki, Hiroaki (2012): Microwave-hydrothermal synthesis of extremely high specific surface area anatase for decomposing NOx, *Ceramics International*, Vol 38, No 8, pp. 6099-6105. https://doi.org/10.1016/j.ceramint.2012.04.057

[4] Sugimoto, Tadao – Zhou, Xingping – Muramatsu, Atsushi (2003): Synthesis of uniform anatase TiO_2 nanoparticles by gel–sol method: 3. *Formation process and size control.* Journal of Colloid and Interface Science, 259(1): 43-52. https://doi.org/10.1016/S0021-9797(03)00036-5

[5] Hirai, T. – Sato, H. – Komasawa, I. (1993): Mechanism of formation of titanium dioxide ultrafine particles in reverse micelles by hydrolysis of titanium tetrabutoxide. *Industrial & Engineering Chemistry Research*, 32(12), 3014-3019. https://doi.org/10.1021/ie00024a009

[6] Noguera, C. (1996): Physics and chemistry at oxide surfaces. *Cambridge University Press*.

[7] Kung, H. H. (1989): Transition metal oxides: surface chemistry and catalysis (Vol. 45). Elsevier.

[8] Erdem, B. – Hunsicker, R. A. – Simmons, G. W. – Sudol, E. D. – Dimonie, V. L. – El-Aasser, M. S. (2001): XPS and FTIR surface characterization of TiO_2 particles used in polymer encapsulation. *Langmuir*, 17 (9), 2664-2669. https://doi.org/10.1021/la0015213

[9] Štengl, V. – Bakardjieva, S. – Murafa, N. (2009): Preparation and photocatalytic activity of rare earth doped TiO_2 nanoparticles. *Materials Chemistry and Physics,* 114(1), 217-226. https://doi.org/10.1016/j.matchemphys.2008.09.025

[10] El-Bahy, Z. M. – Ismail, A. A. – Mohamed, R. M. (2009): Enhancement of titania by doping rare earth for photodegradation of organic dye (Direct Blue). *Journal of Hazardous Materials*, 166(1), 138-143. https://doi.org/10.1016/j.jhazmat.2008.11.022

[11] Keswani, R. K. – Ghodke, H. – Sarkar, D. – Khilar, K. C. – Srinivasa, R. S. (2010): Room temperature synthesis of titanium dioxide nanoparticles of different phases in water in oil microemulsion. *Colloids and Surfaces A: Physicochemical and Engineering Aspects*, 369(1), 75-81. https://doi.org/10.1016/j.colsurfa.2010.08.001

[12] Patil, S. – Kuiry, S. C. – Seal, S. – Vanfleet, R. (2002): Synthesis of nanocrystalline ceria particles for high temperature oxidation resistant coating. *Journal of Nanoparticle Research*, 4(5), 433-438. https://doi.org/10.1023/A:1021696107498

[13] Jin, Y. – Zhu, Y. – Yang, X. – Wei, C. – Li, C. (2007): Fabrication and characterization of cerium-doped titania inverse opal by sol–gel method. *Materials Chemistry and Physics*, 106(2), 209-214. https://doi.org/10.1016/j.matchemphys.2007.05.047

[14] Marimuthu, T. – Anandhan, N. – Rajendran, S. – Mummoorthy, M. – Vidhya, M. (2014): Studies on pure and Ce doped TiO_2 thin films prepared by sol-gel technique. *International Journal of ChemTech Research*, Vol.6, No.13, pp 5309-5314, November 2014

[15] Tong, T. – Zhang, J. – Tian, B. – Chen, F. – He, D. – Anpo, M. (2007): Preparation of Ce–TiO_2 catalysts by controlled hydrolysis of titanium alkoxide based on esterification reaction and study on its photocatalytic activity. *Journal of colloid and interface science*, 315(1), 382-388. https://doi.org/10.1016/j.jcis.2007.06.051

[16] Liu, Z. – Guo, B. – Hong, L. – Jiang, H. (2005): Preparation and characterization of cerium oxide doped TiO_2 nanoparticles. *Journal of Physics and Chemistry of Solids*, 66(1), 161-167. https://doi.org/10.1016/j.jpcs.2004.09.002

[17] Xiao, J. – Peng, T. – Li, R. – Peng, Z. – Yan, C. (2006): Preparation, phase transformation and photocatalytic activities of cerium-doped mesoporous titania nanoparticles. *Journal of Solid State Chemistry*, 179(4), 1161-1170. https://doi.org/10.1016/j.jssc.2006.01.008

[18] Chaisuk, C. – Wehatoranawee, A. – Preampiyawat, S. – Netiphat, S. – Shotipruk, A. – Mekasuwandumrong, O. (2011): Preparation and characterization of CeO_2/TiO_2 nanoparticles by flame spray pyrolysis. *Ceramics International*, 37(5), 1459-1463. https://doi.org/10.1016/j.ceramint.2010.11.018

[19] Wheeler, D. W. – Khan, I. (2014): A Raman spectroscopy study of cerium oxide in a cerium–5wt% lanthanum alloy. *Vibrational Spectroscopy*, 70, 200-206. https://doi.org/10.1016/j.vibspec.2013.12.006

Ref.:
Torres-Romero, A. – **Cajero-Juárez**, M. – **Contreras-García**, M. E. : *Titania-Ceria surfactant assisted sol-gel synthesis and characterization*
Építőanyag – Journal of Silicate Based and Composite Materials, Vol. 69, No. 1 (2017), 8–11. p.
http://dx.doi.org/10.14382/epitoanyag-jsbcm.2017.2

Szol-gél eljárás jellegzetességei titándioxid és cériumdioxid alapanyag szintézisével

Titándioxid nano-részecskék fontos szerepet töltenek be a katalízisben ésa napenergia hasznosításban, sok egyéb más területtel együtt. A cériumdioxid egy ritkaföldfém vegyület amelyet elsősorban fotolumineszcens anyagként, fényérzékeny anyagok előállítása során hasznosítanak. Napjainkban a szol-gél eljárás egy népszerű módszer mezopórusos anyagok előállítására. A cikk bemutatja anatáz fázisú titándioxid-cériumdioxid nanorészecskék előállítását szol-gél eljárással, amelynek során a kiindulási prekurzorok titánbutoxid és cérium-nitrát-hexahidrát. A hőkezelés hőmérséklete 600 °C, sebessége 3 °C min^{-1}, a hőntartás időtartama 2 óra volt. TEM és XRD vizsgálatokon keresztül figyelhetjük meg az elkészült termék jellegzetességeit. Azeredmények igazolják, hogy a CeO_2 beépül a TiO_2 szerkezetbe.
Kulcsszavak: nanorészecskék, titán, cérium, mikroemulzió, szol-gél

european cement research academy

Our mission is to advance innovation in the cement industry within the context of sustainable development and to communicate the latest knowledge and research findings in cement and concrete technology.

With a membership of over 40 leading cement producers worldwide, ECRA supports and conducts research activities on the production of cement and its application in concrete.

ECRA's seminar programme provides a range of pan-European seminars and workshops covering the issues of major importance to the cement industry today.

The European Cement Research Academy (ECRA) was founded in 2003 as a platform on which the European cement industry supports, organises and undertakes research activities within the context of the production of cement and its application in concrete. By creating and disseminating knowledge from research findings, ECRA's aim is to facilitate and accelerate innovation to guide the cement industry.

ECRA's activities are pre-competitive and comprise seminars, workshops and dedicated research projects. Its seminars and workshops provide a platform for teaching the latest knowledge on cement and concrete technology and for communicating and discussing the latest research findings. The seminar programmes cover process and concrete-oriented issues of high concern to the cement industry. Some seminars are of specific interest to cement producers, while others provide information more important to cement associations.

ECRA understands itself as part of a network which comprises various research facilities such as universities, federal institutes and the research centres of cement companies or equipment suppliers. In this context it is able to develop a knowledge centre which benefits from cooperation with the best institutes in the respective areas of research and acts as a core competence centre providing a broad platform for top researchers in each field.

The Academy is steered by a Technical Advisory Board staffed with representatives from major European cement producers under the chairmanship of Daniel Gauthier of HeidelbergCement. The Board is responsible for defining the focus and scope of ECRA's seminar programmes and research projects and monitors the Academy's finances.

ECRA
European Cement Research Academy GmbH
Tannenstrasse 2, 40476 Duesseldorf, Germany
info@ecra-online.org · www.ecra-online.org

The effect of the alkaline solution content on the mechanical properties of MK-based PVA fiber-reinforced geopolymers

Paulo H. R. Borges ▪ Department of Civil Engineering, Faculty of Applied Science, The University of British Columbia
Aamer Bhutta ▪ Department of Civil Engineering, Faculty of Applied Science, The University of British Columbia
Luiggi Teixeira Bavuzo ▪ Department of Civil Engineering, Federal Centre for Technological Education of Minas Gerais (CEFET-MG)
Nemkumar Banthia ▪ Department of Civil Engineering, Faculty of Applied Science, The University of British Columbia

Érkezett: 2016. 12. 13. ▪ Received: 13. 12. 2016. ▪ http://dx.doi.org/10.14382/epitoanyag-jsbcm.2017.3

Abstract
This paper studied the effect of the activation solution content on the mechanical properties of PVA fiber-reinforced geopolymers based on the activation of Metakaolin. Different fiber content (0%, 1% and 2% vol.) of PVA fibers was used to reinforce matrices with different composition (SiO_2/Al_2O_3 molar ratios, i.e. 3.0, 3.4 and 3.8). The amount of activation solution was adjusted to maintain same workability for all fresh mixes and account for the fiber addition. The properties assessed were compressive and flexural strength; capillary sorption tests were used to estimate the durability of the composites. Results show that adjustments in the content of the activation solution slightly reduce the mechanical strength of geopolymers. Nonetheless, as the amount of activation solution increases in the mixes, so does the toughness of the PVA-reinforced composites, which indicates a good correlation between the amount of soluble silica in the fresh geopolymers and mechanical properties in bending.
Keywords: Mechanical properties; durability; metakaolin; geopolymers; fiber reinforced geopolymer composite; PVA fiber; sodium silicate solution

Prof. Paulo H. R. Borges
is an Assistant Professor at CEFET-MG (Federal Centre for Tech. Education of Minas Gerais, Brazil). He has a PhD in Engineering Materials from the University of Sheffield, U.K., on the durability of cementitious materials. His current research is focused on the development of sustainable construction materials, mainly alternative binders to Portland cement.

Dr. Aamer Bhutta
is currently a Research Associate at the Department of Civil Engineering, Faculty of Applied Sciences at UBC. He has received PhD in Civil Engineering from Nihon University, Tokyo in 1995. He has been an Associate Professor in Faculty of Civil Engineering, and a senior fellow at Construction Research Centre (CRC), Universiti Teknologi Malaysia (UTM) from 2009 to 2013. His current research is focused on the development of alternative construction materials, also known as geopolymers.

Luiggi Teixeira Bavuzo
is a civil engineer and M.Sc. candidate at CEFET-MG, working on the development of high performance geopolymer matrices with the addition of short PVA fibers.

Prof. Nemkumar Banthia
is a Professor of Civil Engineering, Distinguished University Scholar and a Canada Research Chair at the University of British Columbia, Vancouver, Canada. Dr. Banthia obtained his Ph.D. from the University of British Columbia in 1987 on Impact Resistance of Concrete, and since then he has been actively pursuing research in the areas of cement-based and polymer-based fiber reinforced composites, with particular emphasis on testing and standardization, fracture behavior, strain-rate effects, durability and development of sustainable materials

1. Introduction

Alkali-activated materials (AAM) are used for many applications, including binding materials for mortars and concretes; they may present several advantages to Portland cement (PC), such as early strength development [1], superior chemical [2-4] and thermal durability [5-6] as well as low carbon emissions [7-8]. AAM are as brittle as PC matrices; therefore, they also require fiber reinforcement to improve deformation, toughness and crack growth when subjected to flexion and tension stresses.

A great variety of fibers have been used to develop fiber-reinforced AAM. Poly vinyl alcohol (PVA) fibers are highly stable in alkaline environment and have been used in the development of high-performance Portland-cement composites, especially Engineered Cementitious Composites (ECC), i.e. those presenting strain-hardening behavior and high ductility (strain capacity of about 5%) [9-11]. Recent studies have proved that PVA fibers also present good bond to AAM [12] and may be used to develop composites with improved impact toughness [13] and excellent resistance to freeze-thaw cycling [14]. Short PVA fibers as a single reinforcement or in hybrid systems may be effective to provide deflection-hardening under flexion or strain-hardening behavior of AAM under direct tension [15-18].

Low calcium or calcium-free AAM are also known as geopolymers. The reinforcement of metakaolin (MK)-based geopolymers with short PVA fibers has been little exploited; few studies were focused on dry mixes for extruded concrete [13-14], where a MK alkali-activated matrix initially fixed in composition (SiO_2 / Al_2O_3 = 4.5; Na_2O / Al_2O_3 = 0.8 and H_2O / Na_2O = 6.4) was altered with the addition of pulverized fly ash. Those studies, therefore, do not present the effect of the SiO_2 / Al_2O_3 molar ratio on the mechanical properties and durability of PVA-reinforced composites, despite the fact that this parameter significantly affects the mechanical properties [20].

Many studies on geopolymer also neglect the fact that, from a production perspective, an alkaline solution of fixed composition will be employed and adjustments on its content may the necessary onsite, either to account for the fiber reinforcement or unexpected changes in workability due to ambient conditions or aggregates moisture content. The objective of this paper is to study the mechanical performance of PVA-geopolymer made from the alkaline activation of MK. Densified silica fume (SF) was used in order to alter the composition of the matrices (namely SiO_2 / Al_2O_3 molar ratio) without changing the composition of the activation solution. The amount of alkaline solution is increased to maintain same consistency for all fresh mixes. The mechanical behavior of the composites is discussed in terms of the composition of the matrices as well as the content of the alkaline activator of fixed composition.

2. Materials and methods

2.1 Materials

Commercial MK was supplied by Powerpozz; it has mean particle size of 4.5 μm and chemical composition shown in *Table 1*. Small quantities of SF (*Table 1*) replaced MK as binder. SF contained low percentage of Al_2O_3; therefore, small replacements of MK with SF increased the overall designed SiO_2 / Al_2O_3 molar ratio of the formulations without the need for altering the composition of the activator (another source of SiO_2). The replacement of MK with SF to alter the SiO_2 / Al_2O_3 has been employed elsewhere [21]. The alkaline activators consisted of sodium hydroxide and sodium silicate solutions (Na_2O = 14.7%, SiO_2 = 29.4%; H_2O = 55.9% wt.). A very fine natural river sand was used (sieved to pass 600 μm), which is a common grading for fiber reinforced PVA composites [17-18]. The short PVA fibers were supplied by Kuraray Japan; its geometry and properties are shown in *Table 2*.

Oxides	MK (%)	SF (%)
SiO_2	54.54	95.53
Al_2O_3	44.16	2.48
CaO	-	0.58
Fe_2O_3	0.51	0.16
Na_2O	-	0.10
K_2O	-	1.01
SO_3	-	0.12
TiO_2	0.32	-
Specific gravity	2.5	2.3

Table 1. Chemical composition of MK and SF
1. táblázat MK és SF kémiai összetétele

Type	Diameter (μm)	Length (mm)	Specific gravity (g/cm³)	Tensile Strength (MPa)	Elongation (%)	Young Modulus (GPa)
REC15	40	8	1.3	1600	6	41

Table 2. Properties of PVA fiber
2. táblázat PVA szálak jellemzői

2.2 Preparation of geopolymer composites

Matrices with three different Si_2O_2 / Al_2O_3 molar ratio were produced, equal to 3.0, 3.4 and 3.8; their solution composition (Na_2SiO_3 / NaOH wt. ratio) and molarity of NaOH solution were kept always constant, equal to 1.5 and 8 M, respectively, which gave rise to a fixed R = SiO_2/Na_2O molar ratio in the solution equal to 1.08. The 8-mm PVA fibers were employed at 1% and 2% volume fraction; unreinforced geopolymers were also used as reference matrices. The alkaline solution to binder (MK or MK+SF) ratio was 1.10 in mass for all geopolymers without PVA fiber; that amount of solution provides a consistency of 253-255 mm to the fresh mixes (*Table 3*), according to the flow table test given by BS 1015-3 [22]. The addition of PVA fibers alters the workability of the fresh mixes; so the solution to binder (s/b) was increased to 1.25 and 1.40 for geopolymers with 1% and 2% PVA fibers, respectively, in order to maintain the overall consistency between 253-261 mm. *Table 3* shows the formulations, their mix design and consistency, as well as the activating parameters of the matrices (molar ratios). The formulation codes contain (i) the term MK to designate that the main precursor is metakaolin; (ii) the numbers 3.0, 3.4 or 3.8 to designate the SiO_2/Al_2O_3 molar ratio (obtained from the chemical composition of MK, SF and solids in the activator) and (iii) the terms PVA_1 and PVA_2 to describe the inclusion of either 1% or 2% vol. PVA. It is possible to observe that the s/b ratio increased for mixes with PVA, but the H_2O / Na_2O molar ratio was kept constant (12.8) for all geopolymers. As water does not take place in the alkali reaction, any change in that activating parameter may adversely affect the porosity and transport properties such as permeability. The changes in the activation content, however, affected the Na_2O/SiO_2 and Na_2O/Al_2O_3 molar ratio (*Table 3*), with consequences in the mechanical strength that will be discussed in section 3.1.

The alkaline solutions (Na_2SiO_3 and NaOH) were mixed together on the day of casting to prepare the liquid activator and allowed to cool down before mixing. A Hobart mixer was used for mixing; firstly, the alkaline solution was added, then MK (or MK+SF) was added in small amounts while mixing. This procedure allowed for complete homogenization of the pastes, which were quite sticky. The dried sand (aggregate to binder ratio = 2.0 for all formulations) was subsequently added,

Formulation	PVA % vol.	s/b ratio	Flow table (mm)	s/b ratio	Composition of the alkaline solution			Activating parameters			
					NaOH (M)	Na_2SiO_3/ NaOH (mass)	SiO_2/ Na_2O (molar)	SiO_2/ Al_2O_3	H_2O/ Na_2O	Na_2O/ SiO_2	Na_2O/ Al_2O
MK 3.0	0	1.10	255	1.10	8	1.5	1.08	3.0	12.8	0.25	0.73
MK 3.4	0	1.10	257	1.10	8	1.5	1.08	3.4	12.8	0.25	0.79
MK 3.8	0	1.10	253	1.10	8	1.5	1.08	3.8	12.8	0.22	0.85
MK 3.0_PVA_1	1	1.25	258	1.25	8	1.5	1.08	3.0	12.8	0.27	0.81
MK 3.4_PVA_1	1	1.25	261	1.25	8	1.5	1.08	3.4	12.8	0.26	0.87
MK 3.8_PVA_1	1	1.25	257	1.25	8	1.5	1.08	3.8	12.8	0.25	0.94
MK 3.0_PVA_2	2	1.40	254	1.40	8	1.5	1.08	3.0	12.8	0.29	0.89
MK 3.4_PVA_2	2	1.40	260	1.40	8	1.5	1.08	3.4	12.8	0.28	0.96
MK 3.8_PVA_2	2	1.40	260	1.40	8	1.5	1.08	3.8	12.8	0.27	1.03

Table 3. Formulations studied
3. táblázat Vizsgált összetételek

followed by another 2-3 minutes of mixing for homogenization. The PVA fibers were added at the end of the mixing process and the mortars were mixed for another 5 minutes to ensure proper dispersion of fibers.

The geopolymers were cast in 50 mm cubes for compressive strength, 50 × 100 mm (diameter × height) cylinders for capillary absorption tests and (50 × 50 × 240) mm beams for flexural strength tests. The specimens were cured at 45°C for 24h and subsequently at room temperature for 27 days prior to testing.

2.3 Mechanical Properties

Compressive strength testing was performed after 28 days in conformity with ASTM C39 [23]; four specimens for each formulation were tested and the average and standard deviation reported. The flexural strength was carried out using a third-point loading test according to ASTM C 1609 [24]; mid-span displacement was monitored by means of a Linear Variable Differential Transducer (LVDT) and the load was applied with a servo-hydraulic universal INSTRON machine at standard displacement rate of 0.025-0.075 mm/min. The main parameters calculated as per ASTM C1609 were the flexural first-peak strength, f_1, (Eq. 1), flexural peak strength, f_p, (Eq. 2).

$$f_1 = \frac{P_1 L}{bd^2} \quad (1)$$

$$f_p = \frac{P_p L}{bd^2} \quad (2)$$

Where P_1 and P_p are first-peak load and peak load, respectively, L is the span length (180 mm), b is the average width (~50 mm) of the specimen at the fracture and d is the average depth (~50 mm) of the specimen at the fracture. Four samples of each geopolymer formulation were tested and a representative curve is presented. The average toughness of the composites was also calculated, from the area under the Load × Mid-span deflection curves until imminent fracture of the composites, when the test was stopped.

The estimation of the durability of the FRGC was carried out by capillary sorptivity tests, following the recommendation of ASTM C1585 [25], but using cylindrical samples with other dimension (50 × 100, diameter × height). The test consists of monitoring the gain of weight over time as water passed into the dried sample through capillary suction until 72 h of testing. Five cylinders were used per geopolymer and the average of the capillary sorptivity (g/cm^2) was calculated and plotted against the square root of time. The slope of the curves, known as the coefficient of capillary suction (g/cm^2.h$^{1/2}$) was used as a parameter to estimate the durability of the composites studied.

3. Results and discussion

3.1 Mechanical properties

Fig. 1 shows the compressive strength of the geopolymers. A large standard deviation indicates that the results were quite variable. *Fig. 1a* shows that the PVA fiber inclusion decreased

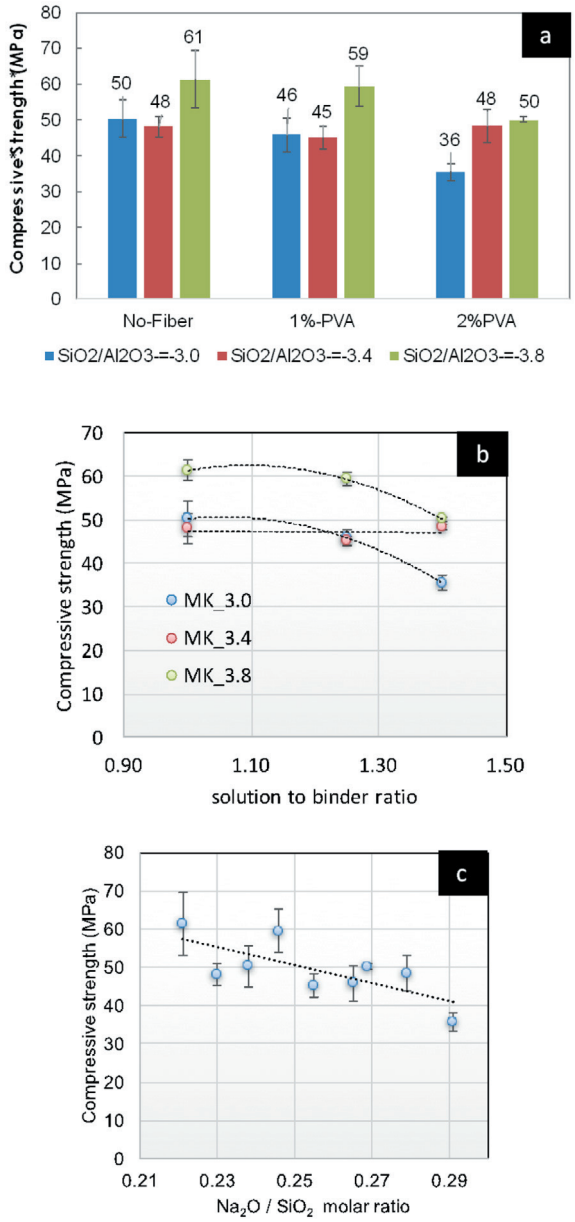

Figure 1. Compressive strength of geopolymers as a function of (a) volume of PVA fibers; (b) activator content; (c) Na_2O/SiO_2 molar ratio.

1. ábra Geopolimerek nyomószilárdsága (a) a PVA száladagolás függvényében, (b) az aktivátor tartalom függvényében, (c) a Na_2O/SiO_2 moláris arány függvényében

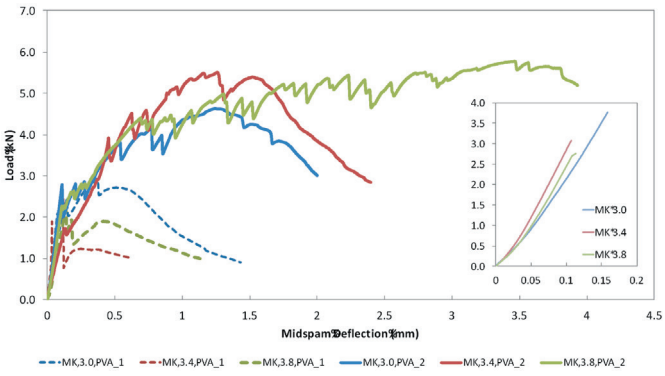

Figure 2. Load (kN) versus mid-spam deflection (mm) curves for MK-based geopolymers

2. ábra Teher (kN) lehajlás (mm) ábrák MK bázisú geopolimerekre

the average compressive strength in MK 3.0_PVA_1 and MK 3.0_PVA_2, compared to their counterpart MK 3.0 (from 50 MPa without fiber to 36 MPa with 2% PVA). The drop in the compressive strength, however, is neither observed in PVA-geopolymers with SiO_2 / Al_2O_3 with 3.4 nor statistically significant in those with SiO_2 / Al_2O_3 = 3.8, despite the remarkable reduction in the average strength from 61 MPa in MK 3.8 to 50 in MK PVA_2. *Fig. 1b* shows that the reduction in strength may be not associated with the fiber addition, but rather with the increase in the amount of solution (s/b from 1.10 to 1.40). In fact, a rise in the solution content to account for the fiber addition corresponds to an increase in the Na_2O/SiO_2 molar ratio in the geopolymers, with consequent reduction in the strength. Indeed, *Fig. 1c* shows that the strength drops when the Na_2O / SiO_2 increases from 0.21 to 0.29, which is the case for the formulations with 1% and 2% PVA (all with Na_2O / SiO_2 > 0.25). It is possible to see that the rise in the s/b from 1.0 to both 1.25 and 1.45 ensured suitable workability for PVA-reinforced geopolymers; however, the higher amount of Na_2O available in the systems also reduced the strength. Previous research [26] has indicated that the optimum Na_2O / SiO_2 molar ratio is approximately 0.25 for higher compressive strength, which is in line with *Fig. 1c*.

The higher strength for MK 3.8 compared to MK 3.0 and MK 3.4 is in accordance with the studies of De Silva et al [30], who found that the compressive strength of MK-based geopolymers increases with higher SiO_2/Al_2O_3 molar ratios varying from 2.5 to 5.0, especially observed at later stages.

Fig. 2 shows the Load (kN) × mid-span (mm) deflection curves for the geopolymer studied after third-point loading tests. The reference formulations (MK 3.0, MK 3.4 and MK 3.8) curves are enlarged in the inset of the graph for clarity. A deflection-hardening behavior was observed for composites reinforced with 2% PVA, i.e. MK 3.0_PVA_2, MK 3.4_PVA_2 and MK 3.8_PVA_2. These composites presented a ratio between the peak strength and first peak strength (f_p / f_1) equal to 1.7, 1.8 and 2.2, respectively, as shown in *Table 4*.

	MK 3.0	MK 3.0 PVA_1	MK 3.0 PVA_2	MK 3.4	MK 3.4 PVA_1	MK 3.4 PVA_2	MK 3.8	MK 3.8 PVA_1	MK 3.8 PVA_2
(f_p/f_1)	1.0	1.5	1.7	1.0	1.0	1.8	1.0	1.0	2.2
Ductility index ($\delta f_p/\delta f_1$)	1.0	3.5	12.0	1.0	1.0	4.8	1.2	1	23.5
Toughness (J)	0	3	8	0	3	10	0	2	20

Table 4. Average f_p / f_1 ratio, ductility index and toughness of the AAM
4. táblázat Átlagos f_p / f_1 arány, duktilitási index és szívósság

Table 4 also presents results of the ductility ratio (δf_p / δf_1) and toughness of the composites. Is it possible to see that the toughness was substantially increased at 2% PVA addition for all geopolymers. *Table 4* shows that an increase from 1% to 2% PVA yielded a toughness 2.7 and 10 times higher for matrices with SiO_2 / Al_2O_3 equal to 3.4 and 3.8, respectively. Indeed, a higher SiO_2 / Al_2O_3 molar ratio increased the deformation and toughness of the PVA-geopolymers: MK 3.8_PVA_2 presented toughness 2.5× and 2× higher and ductility index 2.0× and 4.9x higher than MK 3.0_PVA_2 and MK 3.4_PVA_2, respectively. So, it is possible to observe that a higher SiO_2 / Al_2O_3 has a positive effect in the ductility and toughness of AAM for a fixed PVA percentage equal to 2%. This is also evident on the fractured samples after bending tests (*Fig. 3*). It is possible to observe that the composites with 2% PVA presented several cracks but MK 3.8_PVA_2 was the only one with multi-cracking behavior typical from high-ductile composites.

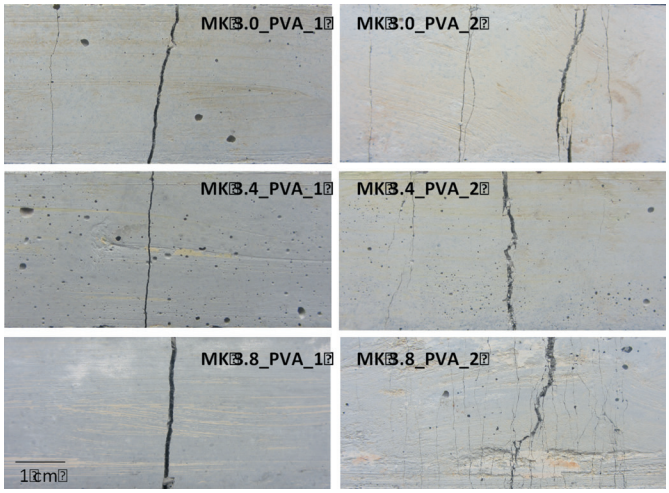

Figure 3. Cracked samples after bending tests
3. ábra Megrepedt próbatestek hajlítóvizsgálat után

Fig. 4 confirms that the improvement in toughness is related not only to the SiO_2 / Al_2O_3 molar ratio but also to the amount of solution in the fresh mixes. Irrespective of the matrix composition, a significant increase in toughness is observed as the solution to binder content increased (*Fig. 4a*), which also corresponds to a rise in the soluble silica content (*Fig. 4b*).

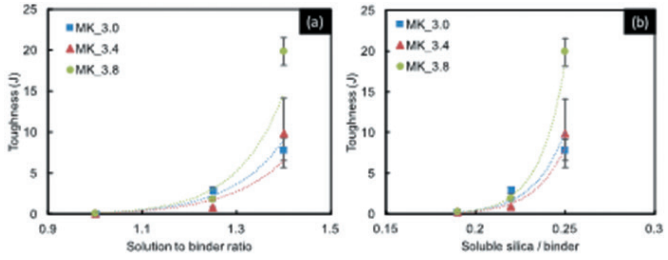

Figure 4. Toughness of the PVA-geopolymer as a function of (a) solution to binder ratio and (b) soluble silica / binder
4. ábra PVA geopolimerek szívóssága (a) az oldat/kötőanyag arány függvényében, (b) az oldható szilika/kötőanyag arány függvényében

3.2. Capillary sorption

Fig. 5 shows the capillary sorption of the geopolymers studied, as well as the coefficient of capillary suction C (g/cm^2.h$^{1/2}$). It is possible to see that the addition of PVA fibers with employment of a higher solution to binder content increased the capillary sorption compared to the plain matrices (*Fig. 5* and *Fig. 6*); this is in line with the compressive strength results, which show a reduction in strength with fiber addition. Nonetheless, the rise in C with the employment of 2% PVA fibers (compared to the unreinforced matrix) is similar for matrices with different SiO_2 / Al_2O_3 molar ratio: 47% in MK 3.0_PVA_2 (0.53 against 0.36 g/cm^2.h$^{1/2}$); 51% in MK 3.4_

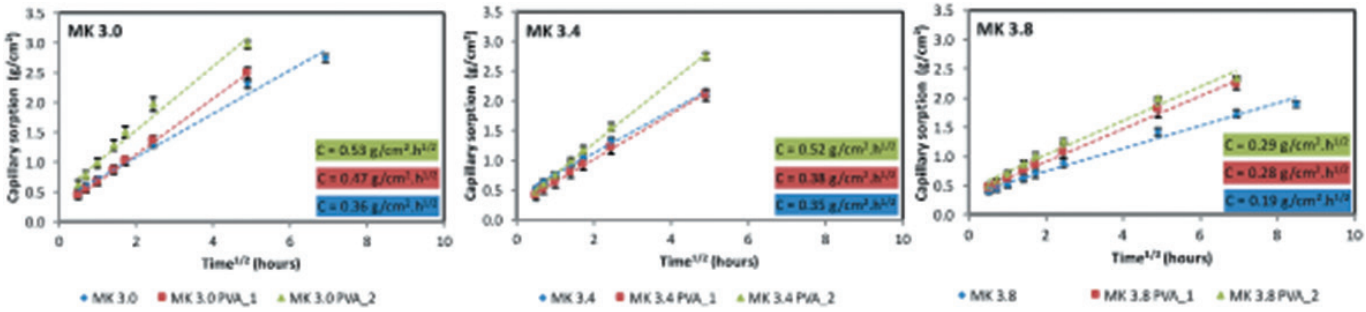

Figure 5. Capillary sorption of AAM studied
5. ábra A vizsgált AAM minták kapilláris szorpciója

PVA_2 (0.52 against 0.35 g/cm².h$^{1/2}$); 53% in MK 3.8_PVA_2 than MK 3.8 (0.29 against 0.19 g/cm².h$^{1/2}$). *Fig. 5* and *Fig. 6* also indicate that the matrix with SiO_2 / Al_2O_3 = 3.8 has reduced capillary sorption when compared to the others matrices with lower ratios, i.e. 3.0 and 3.4. The highest C is 0.29 g/cm².h$^{1/2}$ for MK 3.8_PVA_2, which is even lower than C in unreinforced matrices with SiO_2 / Al_2O_3 = 3.0 and 3.4 (MK 3.0 with C = 0.36 and MK 3.4 with C = 0.35 g/cm².h$^{1/2}$). The results indicate that MK 3.8_PVA_2 is a matrix which not only exhibits better mechanical properties (highest peak strength, f_p/f_1, ductility index and toughness, ~50 MPa compressive strength), but also displays better durability-related properties (lower capillary sorption) among the investigated matrices.

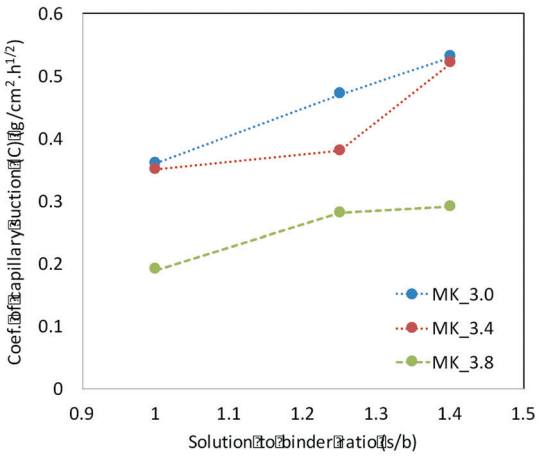

Figure 6. Coefficient of capillary sorption as a function of the solution to binder ratio
6. ábra Kapilláris szorpciós együttható az oldat/kötőanyag arány függvényében

4. Conclusions

This paper studied the mechanical and durability-related properties of unreinforced metakaolin (MK)-based geopolymers with different SiO_2 / Al_2O_3 molar ratios (3.0, 3.4 and 3.8) and also reinforced with short PVA fibers with volume fraction of 1% and 2%. The effect of solution content on the mechanical properties was also discussed. The following conclusions can be drawn:

1. PVA fibers may be used to reinforce MK-based geopolymers; the amount of activating solution, however, needs adjustments as the PVA content increases (herein up to 2%) in order to maintain the workability of the fresh mixes (253-261 mm using the flow table test).
2. The employment of higher solution to binder ratio to account for fiber addition has a slightly negative impact on the average compressive strength and capillary sorption. A rise in the solution content with fixed composition may represent an increase the Na_2O/SiO_2 molar ratio to a level that exceeds the optimum value (0.25) to achieve better mechanical properties.
3. The addition of PVA fibers at 2% vol. allows for the development to geopolymers with deflection-hardening behavior in flexion. Improved toughness and ductility are related not only to the SiO_2 / Al_2O_3 molar ratio but also to the amount of soluble silica in the fresh mixes (i.e. amount of sodium silicate); a significant increase in toughness is observed as the solution to binder content or soluble silica to binder ratio (by mass) increased. The toughness is also higher when a matrix of higher SiO_2 / Al_2O_3 molar raio is designed. Overall it is possible to conclude that the reduced mean strength and higher capillary sorption of geopolymer made with fibers and higher solution content are compensated with better deformation and toughness.

5. Acknowledgements

The financial support of Canada-India Research Center of Excellence (IC-IMPACTS) in this research is highly appreciated. Paulo H. R. Borges would like to thank CNPQ, (Conselho Nacional de Desenvolvimento Científico e Tecnológico), of the Ministry of Science, Technology and Innovation of Brazil for funding his stay at the University of British Columbia, where this research was carried out (grant 201091/2014-3).

References

[1] Fernández-Jiménez, A. M. – Palomo, A. – López-Hombrados, C. (2006): Engineering properties of alkali-activated concrete. *ACI Materials Journal* (103) (2), p. 106-112. https://doi.org/10.14359/15261

[2] Palomo, A. – Blanco-Varela, M. T. – Granizo, M. L. – Puertas, F. – Vazquez, T. – Grutzeck, M. W. (1999): Chemical stability of cementitious materials based on metakaolin. *Cement and Concrete Research* (29), p. 997–1004. https://doi.org/10.1016/S0008-8846(99)00074-5

[3] Bakharev, T. (2005): Resistance of geopolymer materials to acid attack. *Cement and Concrete Research* (35), 658-670. https://doi.org/10.1016/j.cemconres.2004.06.005

[4] Bakharev, T. (2005): Durability of geopolymer materials in sodium and magnesium sulfate solutions. *Cement and Concrete Research* (35) (6), p. 1233-1246. https://doi.org/10.1016/j.cemconres.2004.09.002

[5] Kong, D. L. Y. – Sanjayan, J. G. (2008): Damage behavior of geopolymer composites exposed to elevated temperatures. *Cement and Concrete Composites* (30) p. 986–991 https://doi.org/10.1016/j.cemconcomp.2008.08.001

[6] Kong, D. L. Y. – Sanjayan, J. G. (2010): Effect of elevated temperatures on geopolymer paste, mortar and concrete, *Cement and Concrete Research* (40) (2), p. 334-339. https://doi.org/10.1016/j.cemconres.2009.10.017

[7] McLellan, B. C. – Williams, R. P. – Lay, J. – van Riessen, A. – Corder, G. D. (2011): Costs and carbon emissions for geopolymer pastes in comparison to ordinary portland cement, *Journal of Cleaner Production* (19) (9–10) p. 1080-1090. https://doi.org/10.1016/j.jclepro.2011.02.010

[8] Turner, L. K. – Collins, F. G. (2013): Carbon dioxide equivalent (CO2-e) emissions: A comparison between geopolymer and OPC cement concrete. *Construction and Building Materials* (43), p. 125-130. https://doi.org/10.1016/j.conbuildmat.2013.01.023

[9] Li, V. – Kanda, T. (1998): Innovations Forum: Engineered Cementitious Composites for Structural Applications. *Journal of Materials in Civil Engineering* (10) (66), p. 66-69. https://doi.org/10.1061/(ASCE)0899-1561(1998)10:2(66)

[10] Li, V. C. (1998): Engineered Cementitious Composites – Tailored Composites Through Micromechanical Modeling, In: *Fiber Reinforced Concrete: Present and the Future*, Eds: N. Banthia, A. Bentur, and A. Mufti, Canadian Society of Civil Engineers, 213 p.

[11] Li, V. C. (2003): On Engineered Cementitious Composites (ECC) – A review of the material and its applications. *Journal of Advanced Concrete Technology* (1) (3), p. 215-30.

[12] Li, Z. – Zhang, Y. – Zhou, X. (2005): Short Fiber Reinforced Geopolymer Composites Manufactured by Extrusion. *Journal of Materials in Civil Engineering* (17) (6), p. 624–631. https://doi.org/10.1061/(ASCE)0899-1561(2005)17:6(624)

[13] Zhang, Y. – Sun, W. – Li, Z. (2006): Impact behavior and microstructural characteristics of PVA fiber reinforced fly ash-geopolymer boards prepared by extrusion technique. *Journal of Materials Science* (41) (10), p. 2787-2794. https://doi.org/10.1007/s10853-006-6293-5

[14] Zhang Y. – Sun, W. – Li, Z. – Zhou X. – Eddie, Chau C. (2008): Impact properties of geopolymer based extrudates incorporated with fly ash and PVA short fiber. *Construction and Building Materials* (22) (3), p. 370-383. https://doi.org/10.1016/j.conbuildmat.2006.08.006

[15] Nematollahi, B. – Sanjayan, J. – Uddin, F. – Shaikh, A. (2014): Comparative deflection hardening behavior of short fiber reinforced geopolymer composites. *Construction and Building Materials* (70), p. 54-64. https://doi.org/10.1016/j.conbuildmat.2014.07.085

[16] Nematollahi, B. – Sanjayan, J. – Shaikh, A. F. (2015): Tensile Strain Hardening Behavior of PVA Fiber-Reinforced Engineered Geopolymer Composite. *Journal of Materials in Civil Engineering* 27) (10), p. 5696-5704. https://doi.org/10.1061/(ASCE)MT.1943-5533.0001242

[17] Ohno, M. – Li, V. C. (2014): A feasibility study of strain hardening fiber reinforced fly ash-based geopolymer composites. *Construction and Building Materials* (57), p. 163-168. https://doi.org/10.1016/j.conbuildmat.2014.02.005

[18] Shaikh, F. U. A. (2013): Deflection hardening behavior of short fibre reinforced fly ash based geopolymer composites. *Materials and Design* (50), p. 674-682. https://doi.org/10.1016/j.matdes.2013.03.063

[19] Zhang Y. – Sun W. – Li Z. – Zhou X. (2009): Geopolymer Extruded Composites with Incorporated Fly Ash and Polyvinyl Alcohol Short Fiber *ACI Materials Journal* (106) (1),p. 3-10. https://doi.org/10.14359/56310

[20] Duxson, P. – Provis, J. L. – Lukey, G. C. – Mallicoat, S. W. – Kriven, W. M. – van Deventer, J. S. J. (2005): Understanding the relationship between geopolymer composition, microstructure and mechanical properties. *Colloids and Surfaces A: Physicochemical and Engineering Aspects* (269), p. 47-58. https://doi.org/10.1016/j.colsurfa.2005.06.060

[21] Yunsheng, Z. – Wei, S. – Zongjin, L. (2010): Composition design and microstructural characterization of calcined kaolin-based geopolymer cement, *Applied Clay Science* (47) (3-4), pp. 271-5. https://doi.org/10.1016/j.clay.2009.11.002

[22] BS EN 1015-3, Methods of test for mortar for masonry – Part 3: Determination of consistence of fresh mortar (by flow table), 6 p.

[23] ASTM C39, Standard Test Method for Compressive Strength of Cylindrical Concrete Specimens.

[24] ASTM C 1609, Standard Test Method for Flexural Performance of Fiber-Reinforced Concrete (Using Beam with Third-Point Loading).

[25] ASTM C1585-13 Standard Test Method for Measurement of Rate of Absorption of Water by Hydraulic-Cement Concretes, 6 p.

[26] Barbosa, V. F. – MacKenzie K. J. – Thaumaturgo C. (2000): Synthesis and characterisation of materials based on inorganic polymers of alumina and silica: sodium polysialate polymers. *International Journal of Inorganic Polymers*, (2), p. 309–17.

[27] De Silva, P. – Sagoe-Crenstil, K. – Sirivivatnanon, V. (2007): Kinetics of geopolymerization: Role of Al_2O_3 and SiO_2, *Cement and Concrete Research* (37) (4), pp. 512-8. https://doi.org/10.1016/j.cemconres.2007.01.003

Ref.:
Borges, Paulo H. R. – **Bhutta**, Aamer – **Teixeira Bavuzo,** Luiggi – **Banthia**, Nemkumar: *The effect of the alkaline solution content on the mechanical properties of MK-based PVA fiber-reinforced geopolymers* Építőanyag – Journal of Silicate Based and Composite Materials, Vol. 69, No. 1 (2017), 13–18. p. http://dx.doi.org/10.14382/epitoanyag-jsbcm.2017.3

Lúgos oldat tartalom hatása PVA szálerősítésű MK bázisú geopolimerek mechanikai jellemzőire

A cikk bemutatja PVA szálerősítésű, aktivált metakaolin bázisú geopolimerek mechanikai tulajdonságait az aktiváló oldat tartalom változtatásának hatására. Az alkalmazott PVA száltartalom 0 V%, 1 V% és 2V % volt. A vizsgált geopolimerek SiO_2/Al_2O_3 moláris hányada 3,0-3,4-3,8 volt. Az aktiváló oldat mennyiségét úgy választották meg, hogy a friss keverékek bedolgozhatósága azonos legyen mindegyik száltartalom esetén. Vizsgált jellemzők: nyomószilárdság, hajlító-húzószilárdság, kapilláris vízfelvétel (tartóssági jellemzők becslésére). A vizsgálatok kimutatták, hogy az aktiváló oldat mennyiségének hatása van a mechanikai jellemzőkre. Az aktiváló oldat mennyiségével arányosan változott a geopolimerek szívóssága, és az oldható szilika tartalom jó korrelációt mutatott a hajlítóvizsgálatokból megkapható mechanikai jellemzőkkel.
Kulcsszavak: Mechanikai jellemzők; tartósság; metakaolin; geopolimer; szálerősítésű geopolimer kompozit; PVA szál; nátronvízüveg oldat

NANORA

Nano Regions Alliance

NANORA – Nano Regions Alliance is a transnational cooperation network of strong European nanotechnology regions. Its members are regional or national organisations – clusters, technology transfer and business development agencies, industry associations, research and technology centres and the like – that are active in **supporting nanotechnology research and business activities** by implementing regional support programmes and offering services to small and medium companies and/or research institutions. Having started out as a funded INTERREG project (2011-2015) under the lead of the Hessen Ministry of Economics NANORA now, as of mid-2016, counts **17 Members** from Germany, France, Belgium, Ireland, the United Kingdom, the Netherlands, Poland, Spain and Sweden. As of early 2016 high-ranking political decision-makers from several involved regions (Wallonie, BE; Hessen, DE; Saarland, DE; Nord-Pas de Calais, FR; Ireland; North-West England) have pledged their support to the network and its objectives, making support to nanotechnology SMEs a political priority.

Interreg IVB

Investing in Opportunities

This project has received European Regional Development Funding through INTERREG IV B.

INTERREG IVB

Project financed by Interreg IVB North West Europe.

More information:

www.nanora.eu

Dr. David Eckensberger
Project Director Hessen-Nanotech
Konradinerallee 9
65189 Wiesbaden
Germany

info@hessen-nanotech.de

Raman shift of silicon rubber-nano titania PMNC

Sabah Mohammed Mlkat AL MUTOKI ▪ Electrical Department, Al-Furat Al-Awsat University, Technical Institute of Samawa ▪ asabah_sh2003@yahoo.com

Baydaa Abdul-Hassan Khalaf AL-GHZAWI ▪ Mechanical Department, Al-Furat Al-Awsat University, Technical Institute of Samawa ▪ baydaafawz@gmail.com

Samir M. ABDUL AMOHSIN ▪ Physical Department, Faculty of Science, Thi Qar University ▪ samir.mahdi75@gmail.com

Emad A. Jaffar AL-MULLA ▪ College of Health and Medical Techniques, Al-Furat Al-Awsat Technical University ▪ emadalmulla@atu.edu.iq

Érkezett: 2016. 12. 14. ▪ Received: 14. 12. 2016. ▪ http://dx.doi.org/10.14382/epitoanyag-jsbcm.2017.4

Abstract

Raman shift, FTIR spectra and SEM were used to detect the percolation threshold of nano titania filler ceramic $nTiO_2$ dispersed in a silicon rubber matrix SR8100 by hot vibrate dispersion. It has been found that an additional frequencies, and stock lines appears in Raman shift when $nTiO_2$ reach (5)wt% which mean a change in polarity of the SR8100/$nTiO_2$ PMNC polarity.

Keywords: PMNC, nano ceramic oxide fillers, $nTiO_2$, Raman shift

Sabah Mohammed Mlkat Al Mutoki
is an Assist. Prof. at Al-Furat Al-Awssat Technical University, Iraq. He is the dean of Al Samawah Technical Institute since 2014. He got his PhD from Lancaster University, UK, 2012, in the field of condensed materials nano-technology. Interest in: nano-materials, nano-composites, electronic applications of nano-materials.

Baydaa Abul Hassan Khalaf Al Ghazawi
is a lecturer at Al Samawah Technical Institute, Al-Furat Al-Awssat Technical University. She has her Master degree in ceramic technology from Baghdad Technical College, The Middle Technical University at 2007, currently she is a PhD student.

Samir M. Abdulalmohsin
is an Asst. Prof. at University of Thi Qar, Faculty of Science, Department Of Physics, Iraq; University ; He has received his Ph.D. from University of Arkansas at Little Rock (UALR) in 2014. Main fields of interest: Applied Physics, Opto Electronics, Nanostructure Materials, Solar Cells. He has more than 20 papers with citation about 78.

Emad Abbas Jaffar Al-Mulla
is an Asst. Prof. College of Health and Medical Techniques, Al-Furat Al-Awsat Technical University, Iraq; He has received his PhD from Universiti Putra Malaysia, Malaysia in 2010, He was a Postdoctoral researcher at the same University from April 2012 to April 2013; main fields of interest: bioorganic synthesis, nano-materials, biopolymer nano-composites; He has more than 50 papers in Scopus and ISI journals; his H-Index = 14 according to Scopus database.

1. Introduction

It is increasingly being recognized that new applications for materials require functions and properties that are not achievable with single materials. In this sense, composites formed by a polymer matrix and a conductive nano second phase are very interesting materials [1], these conducting polymer matrix nano composites PMNCs are capable of dissipating electrostatic charges and shielding devices from electromagnetic radiation [2]. Dielectric property of PMNCs with different conductivity fillers, such as carbon nano tube (CNT), cupper (Cu) and nickel (Ni) powders was investigated by several researchers [2-5]. Dependence of the dielectric property of the PMNC composites on frequency and volume fraction of fillers was also studied [6,7]. With gradually increasing the conducting filler content, composites undergo a percolation transition where the electrical conductivity of the composite jumps up several orders of magnitudes and its nature changes from an insulator to a conductor. This behavior is attributed to the formation of conducting network through the insulating matrix material when the filler content is at or above the percolation threshold [8,9]. The critical content of any filler that characterizes a drastic increase in conductivity is commonly termed as the electrical percolation threshold (EPT) [10]. On the other hand the use of nano ceramic oxides as a filler in several polymer matrixes can be viewed as one of the most promising area driven towards electronic applications [11]. Among all the ceramic oxide nano fillers $nTiO_2$ is documented to have the highest effect on the PMNCs, especially on the electrical and thermal properties. The improvement in these properties observed for $nTiO_2$ filled polymers could be due to one and/or more of the following factors (i) the large surface area of nano particles which creates a large interaction zone or region of altered polymer behavior, (ii) change in the polymer morphology due to the surfaces of nano particles, (iii) a reduction in the internal field caused by the decrease in the size of the particles, (iv) change in the space charge distribution, (v) scattering mechanism [12-17]. Aim of this research was to determine the percolation threshold of a new PMNC composed of SR8100 and $nTiO_2$ ceramic filler fabricated by hot vibrate dispersion (HVD).

2. Experiments

2.1 Materials

SR8100 polymer containing resin and hardener from (SICOMEN, USA), and (99.9%), and (10 nm) TiO_2 from (HORIBA, Germany).

2.2 Method

Polymer matrix discs were prepared using mould with 1cm diameter and 1cm height, the ratio of resin and hardener was 1:3. They were stirred by a magnetic stirrer for 5 min, then it was purred into the mould leaving for 24 hrs. After solidification the polymer discs were put in 1×1 cm cylindrical mould with a moving base with TiO_2 nano powder. The mould was then heated up to 80 °C and vibrate ultrasonically for 1 hr to ensure a uniform disperse for TiO_2 nano particles in SR8100 polymer matrix. Then it was left to cool down at room temperature.

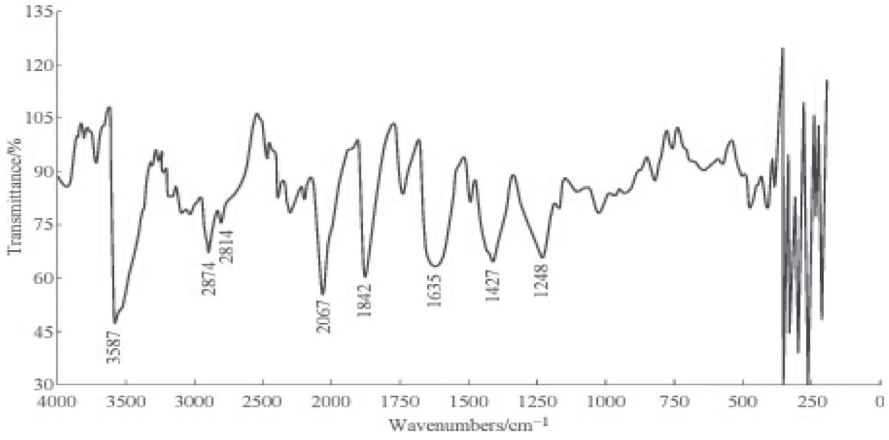

Fig. 1 FTIR of SR8100/nTiO$_2$ PMNCs
1. ábra SR8100/nTiO$_2$ PMNC FTIR spektruma

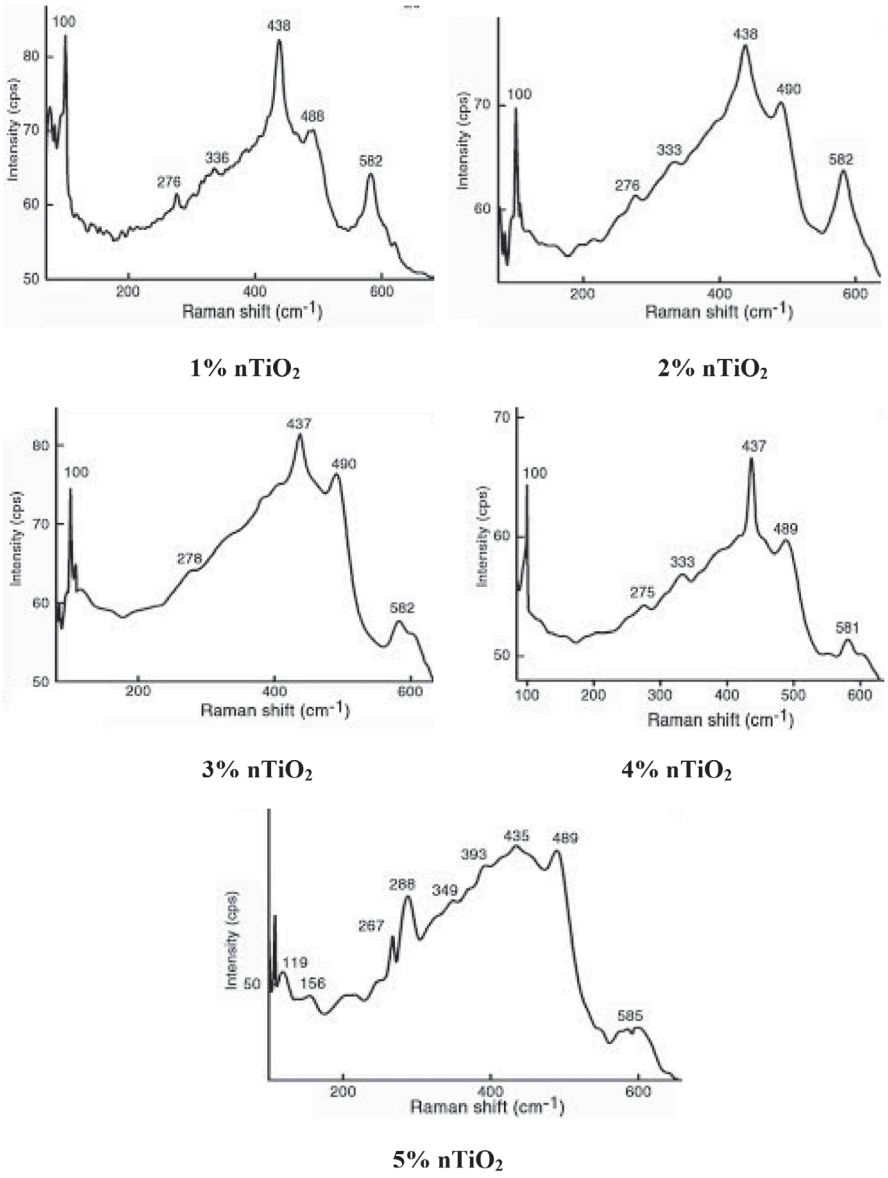

Fig. 2 Raman Shift of SR8100/nTiO$_2$ PMNCs
2. ábra SR8100/nTiO$_2$ PMNC Raman eltolódása

Specimens were tested by Raman shift, FTIR, and SEM to detect their properties.

3. Results and discussion

In the present work we succeeded to change polarity of silicon rubber (SR8100) by the addition of nano titania filler with 10 nm particle size using hot vibrate dispersion technique to prepare a polymer matrix nano composite material (PMNC) with high electrical conductivity. Both heating and vibrating used in PMNC preparation stimulate molecules and give it the energy it need to vibrate and spin creating a large change in the polarity of the polymer matrix as we shall see from Raman shift of the SR8100/nTiO$_2$ PMNC specimen. *Fig. 1* illustrates FTIR of SR8100/TiO$_2$ PMNC. PMNC specimen peaks at (1472.32,1635.64) refers to phases where SR8100 epoxy is the dominant, while peaks at (3587.60, 3525.88, 3464.15) are places where nTiO$_2$ concentrate [20].

Fig. 2 illustrates the Raman shift of SR8100 1-5 wt% nTiO$_2$. It is easy to notice the additional frequencies in Raman shift related to the internal energy of the SR8100/nTiO$_2$ PMNC especially when nTiO$_2$ weight percent is 5% as can be seen from *Fig. 1*, where stock lines has also appeared which is a very interesting result that we shall relay for our future work. From *Fig. 1* we may see the large similarity between Raman shift for the 1-4 wt% nTiO$_2$ PMNC specimen, while the 5 wt% nTiO$_2$ has much different peaks which may refer to a percolation threshold phenomena. According to this fact we may distinguish two types of Raman shift peaks; (i) the repeated peaks that appear in SR8100/nTiO$_2$ PMNC specimen with 1-4 wt% nTiO$_2$, which are as follow, peak at (100) which is related to symmetric stretching of C=O, (275,267 and 278) peaks indicate the stretching mode of C-H bond, (333,336) refer to a combination of C-O stretching and O-H deformation, peaks at 437,438 refer to nTiO$_2$, and/or stretching mode of saturated C-O, it may also refer to a slight entrance between SR8100 polymer matrix and nTiO$_2$ filler. Peaks (488,489,490) all refer to the presence of nTiO$_2$ phase, while (552,581,582,585) peaks indicate the deformation of C-H and C-O-H, ring deformation of polymer matrix and nTiO$_2$ presence [18,19]. Raman shift of 5 wt% nTiO$_2$ shows completely different

peaks than the other SR8100/$nTiO_2$ PMNC specimens. In this specimen $nTiO_2$ is more obvious in the peaks (256,267,288), peak (349) refer to combination of C-O stretching and C=H deformation, peak (393) refers to $nTiO_2$ [20,21], and/or combination of C-O stretching and O-H deformation. Peak (435) indicates stock line that is not defined as polymer or $nTiO_2$; it may indicate percolation threshold and tunneling effect [18] that may take place within SR8100/$nTiO_2$ PMNC. Finally (585) peak refers to $nTiO_2$ and/or deformation of C-C and C-O [19,22,23]. The Raman shift results of this work are in agreement with FTIR results shown in *Fig. 1*.

Fig. 3 illustrates SEM of SR8100/$nTiO_2$ (PMNCs). We can see the good dispersion and high interaction between polymer matrix and nano reinforcing particles; this may lead us to conclude that there is, we may notice that at ultra low $nTiO_2$ concentration 1-3 wt% $nTiO_2$ there is no obvious pattern for dispersion of $nTiO_2$ in SR8100 matrix, hence no percolation is expected. But this regular pattern starts to appear at 4% $nTiO_2$ and continue with the same regular dispersion especially at 5% $nTiO_2$ which gives a very regular dispersion of $nTiO_2$ phase through the SR8100 matrix.

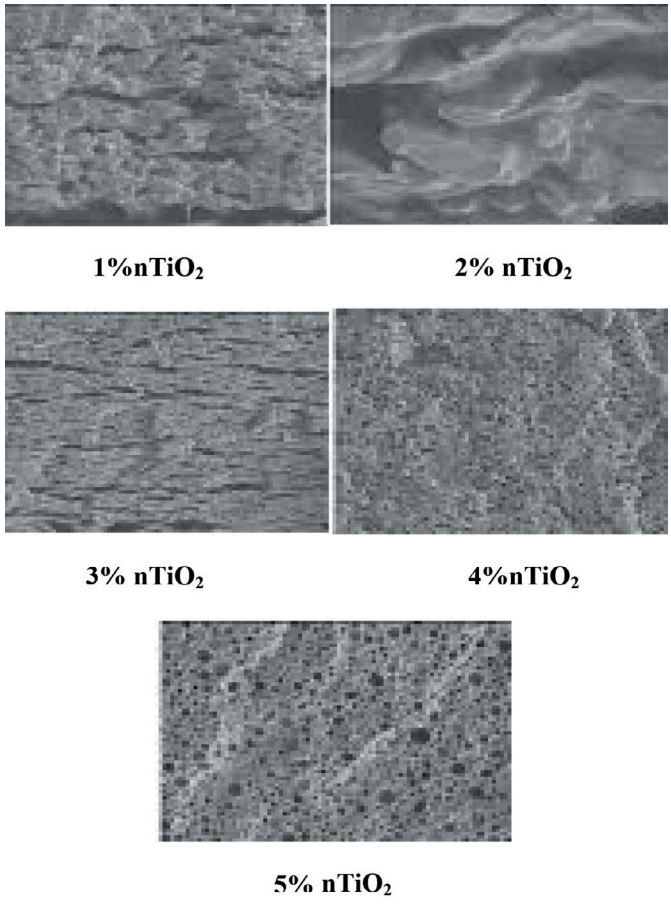

Fig. 3 SEM of SR8100/$nTiO_2$ PMNCs 1-5 wt% $nTiO_2$
3. ábra SR8100/$nTiO_2$ PMNC (1-5 wt% $nTiO_2$) pásztázó elektronmikroszkópos felvételei

Values of electrical resistivity, and thermal conductivity of the SR8100/$nTiO_2$ are listed in Table 1. From the table we may notice that addition of $nTiO_2$ effects on both electrical resistivity, and thermal conductivity when concentration of nano titania filler exceed 3%.

4. Conclusions

Raman shift, FTIR spectra and SEM were used to detect the percolation threshold of nano titania filler ceramic $nTiO_2$ dispersed in a silicon rubber matrix SR8100 by hot vibrate dispersion. It has been found that an additional frequencies, and stock lines appears in Raman shift when $nTiO_2$ reach (5) wt% which mean a change in polarity of the SR8100/$nTiO_2$ PMNC polarity.

Specimen Composition	Electrical Resistivity (Ω.cm)	Thermal Conductivity (W/m.k)
SR8100	1.0×10^{13}	0.120
SR8100+1%$nTiO_2$	0.821×10^{13}	0.416
SR8100+2%$nTiO_2$	3.07×10^{12}	1.002
SR8100+3%$nTiO_2$	5.48×10^{10}	2.714
SR8100+4%$nTiO_2$	2.36×10^{10}	5.227
SR8100+5%$nTiO_2$	4.65×10^{8}	7.186

Table 1..Electrical Resistivity and Thermal Conductivity of SR8100/$nTiO_2$
1. táblázat SR8100/$nTiO_2$ elektromos ellenállása és hővezetési tényezője

References

[1] Yan, T. – Shen, Z. G. – Zhang, W. W. – Chen, J. F. (2006): Size dependence on the ferroelectric transition of nanosized BaTiO3 particles. *Materials Chemistry and Physics*, Vol. 98, pp. 450-455. https://doi.org/10.1016/j.matchemphys.2005.09.058

[2] Wada, S. – Hoshina, T. – Yasuno, H. – Ohishi, M. M. – Kakemoto, H. – Tsurumi, T. – Yashima M. (2013): Size effect of dielectric properties for barium titanate particles and its model. *Key Engineering Materials*, Vol. 301, pp. 27-30. https://doi.org/10.4028/www.scientific.net/KEM.301.27

[3] Caseri, W. R. (2006): Nanocomposites of polymers and inorganic particles: preparation, structure and properties. *Materials Science and Technology*, Vol. 22, pp. 807-817. https://doi.org/10.1179/174328406X101256

[4] Jing Li – Peng Cheng Ma – Chow Wing Sze – To Chi Kai – Ben Zhong Tang – Jang-Kyo Kim (2007): Percolation Threshold of Polymer Nnnocomposites Containing Graphite Nano Platelets and Carbon Nanotubes, *16th International Conference on Composite Materials*, Kyoto-Japan, 2007.

[5] B. H. Kim – J. H. Ahn – J. H. Jeong – Y. S. Jeon – K. O. Jeon – K. S. Hwang (2006): Preparation of TiO_2 Thin Film on SiO_2 Glass by a Spin Coating—*Pyrolysis Process, Ceramics International*, Vol. 32, pp. 223-225. https://doi.org/10.1016/j.ceramint.2005.01.016

[6] Salahuddin Sayeef, Datta, D. – Srivastava, P. – Datta Supriyo (2007): Quantum Transport Simulation of Tunneling Based Spin Torque Transfer (STT) Devices: Design Trade offs and Torque Efficiency, *Electron Devices Meeting*, 2007. IEDM 2007. IEEE International, pp.121-124.

[7] Moya, J. S. – Lopez-Esteban, S. – Pecharroman, C. (2007): The challenge of ceramic/metal microcomposites and nanocomposites. *Progress in Materials Science*. Vol. 52, pp. 1017-1090. https://doi.org/10.1016/j.pmatsci.2006.09.003

[8] Al-Shemmari, F. A. – Rabah, A. A. A. – Al-Mulla, E. A. J. (2014): Comparative study of different Msurfactants for natural rubber clay nanocomposite preparation. *Rendiconti Lincei Scienze Fisiche e Naturali,* Vol. 25, pp. 409-413.

[9] Fahrenholtz, W. G. – Ellerby, D. T. – Loehman, R. E. (2000): Al_2O_3–Ni Composites with high strength and fracture toughness. *Journal of the American Ceramic Society*. Vol. 83, pp. 1279-1280. https://doi.org/10.1111/j.1151-2916.2000.tb01368.x

[10] Tuan, W. H. – Wu, H. H. – Yang, T. J. (1995): The preparation of Al_2O_3/Ni composites by a powder coating technique. *Journal of Materials Science.* Vol. 30, pp. 855-859. https://doi.org/10.1007/BF01178417

[11] Wang, X. – Padture, N. P. – Tanaka, H. (2004): Contact-damage-resistant ceramic/single-wall carbon nanotubes and ceramic/graphite composites. *Nature Materials*. Vol. 3, pp. 539-544. https://doi.org/10.1038/nmat1161

[12] Cho, J. – Boccaccini, A. R. – Shaffer, M. S. P. (2009): Ceramic matrix composites containing carbon nanotubes. *Journal of Materials Science*. Vol. 44, pp. 1934-1951. https://doi.org/10.1007/s10853-009-3262-9

[13] Efros, A. L. – Shklovskii, B. I. (1976): Critical behaviour of conductivity and dielectric constant near the metal-non-metal transition threshold. *Physica Status Solidi B*. Vol. 76, pp. 475-485. https://doi.org/10.1002/pssb.2220760205

[14] Nan, C. W. – Shen, Y. – Ma, J. (2010): Physical properties of composites near percolation. *Annual Review of Materials Research*. Vol. 40, pp. 131-151. https://doi.org/10.1146/annurev-matsci-070909-104529

[15] Bauhofer, W. – Kovacs, J. Z. (2009): A review and analysis of electrical percolation in carbon nanotube polymer composites. *Composites Science and Technology*. Vol. 69, pp. 1486-1498. https://doi.org/10.1016/j.compscitech.2008.06.018

[16] S. F. Chen – J. P. Li – K. Qian – W. P. Xu – Y. Lu – W. X. Huang – S. H. Yu (2010): Large Scale Photochemical Synthesis of M@TiO_2 Nanocomposites (M = Ag, Pd, Au, Pt) and Their Optical Properties, CO Oxidation Performance, and Antibacterial Effect, *Nano Research*, Vol. 3, pp. 244-255. https://doi.org/10.1007/s12274-010-1027-z

[17] Kim, H. J. – Lee, S. M. – Oh, Y. S. – Yang, Y. H. – Lim, Y. S. – Yoon, D. H. (2014): Unoxidized graphene/alumina nanocomposite: fracture and wear-resistance effects of graphene on alumina matrix. *Scientific Reports*. Vol. 4, Article number 5176. https://doi.org/10.1038/srep05176

[18] Fan, Y. C. – Jiang, W. – Kawasaki, A. (2012): Highly conductive few-layer graphene/Al2O3 nanocomposites with tunable charge carrier type. *Advanced Functional Materials*. Vol. 22, pp. 3882-3889. https://doi.org/10.1002/adfm.201200632

[19] Wang, D. – Zhou, T. – Zha, J. W. – Zhao, J. – Shi, C. Y. – Dang, Z. M. (2013): Functionalized graphene–$BaTiO_3$/ferroelectric polymer nanodielectric composites with high permittivity, low dielectric loss, and low percolation threshold. *Journal of Materials Chemistry A*. Vol. 1, pp. 6162-6168. https://doi.org/10.1039/C3TA10460E

[20] Lucía Fernández-García – Marta Suárez – José Luis Menéndez – Carlos Pecharromán – Rosa Menéndez – Ricardo Santamaría (2015): Dielectric behavior of ceramic–graphene composites around the percolation threshold. *Nanoscale Research Letters*, Vol. 10, pp. 216-223. https://doi.org/10.1186/s11671-015-0921-4

[21] Al-Mutoki, S. M. M. – Al-Ghzawi, B. A. H. K. – Al-Mulla, E. A. J. – AbdulAmohsin, S. (2016): Enhancement of Mechanical Properties of Polyamide Hexaglycol by Dispersion of TiO_2 Nanofiller. Nano Biomedicine and Engineering, Vol. 8, pp. 55-59. https://doi.org/10.5101/nbe.v8i2.p55-59

[22] Al-Mutoki, S. M. M. – Wadday, A. G. – Abdullah, A. A. Al-Ghzawi, B. A. K. – Al-Mulla, E. A. J. (2016): Effect of nanoTiO2 dopant on electrical properties of SR8100/nanoTiO_2 PMNC. Results in Physics, Vol. 6, pp. 551–553. https://doi.org/10.1016/j.rinp.2015.12.006

[23] Al-Mutoki, S. M. M. – Al-Ghzawi, B. A. H. K. – Abdullah, A. A. – AlAmmar, A. I. R. – Al-Mulla, E. A. J. (2015): Synthesis and characterization of new epoxy/titanium dioxide nanocomposite. *Nano Biomedicine and Engineering*, Vol. 7, pp. 135-138. https://doi.org/10.5101/nbe.v7i4.p135-138

Ref.:
Al Mutoki, Sabah Mohammed Mlkat – **Al-Ghzawi**, Baydaa Abdul-Hassan Khalaf – **Abdul Amohsin**, Samir M. – **Al-Mulla**, Emad A. Jaffar: *Raman shift of silicon rubber-nano titania PMNC*
Építőanyag – Journal of Silicate Based and Composite Materials, Vol. 69, No. 1 (2017), 20–23. p.
http://dx.doi.org/10.14382/epitoanyag-jsbcm.2017.4

Szilikon gumi-nano titándioxid PMNC Raman eltolódása

A szerzők nanoszemcsés TiO_2 töltőanyagot alkalmaztak SR8100 szilikon gumi ágyazóanyagban. A kialakuló struktúrát és az anyagjellemzőket pásztázó elektronmikroszkóppal, Raman spektroszkópiával és Fourier-transzformációs infravörös spektroszkópiával vizsgálták, és meghatározták az FTIR spektrumokat és a Raman eltolódást a perkolációs határ azonosítása érdekében. Az eredmények rámutattak, hogy 5 m% TiO_2 töltőanyag tartalom felett megváltozik a kompozit polaritása és Raman eltolódása.
Kulcsszavak: PMNC, nano kerámia oxid töltőanyag, nTiO_2, Raman eltolódás

The electrochemical effect of different temperatures on sodium saccharine in blood medium using modified working electrode CNT/GCE by cyclic voltammetry

Muhammed Mizher Radhi
Professor, Department of Radiological Techniques, Health and Medical Technology College-Baghdad, Middle Technical University, Baghdad, Iraq. He received his PhD from University Putra of Malaysia (UPM) in 2010 in Electrochemistry, Nanotechnology. Research topics: conductivity of grafted polymer with nano-deposit and fabrication of sensors by nanomaterials to study drugs in blood medium by electrochemical analysis.

Yousif A. Kadium
Assistant professor, Department of Chemistry, Science College, University of Al-Mustansiriyah, Baghdad, Iraq. Ph.D. from University of Baghdad, Science College, Chemistry Department. Fields of interest: physical chemistry, electrochemistry, surface chemistry.

Anfal Ismael Ibrahim
Ph.D. student at Department of Chemistry, Science College, University of Al-Mustansiriyah, Baghdad, Iraq. Fields of interest: physical chemistry, electrochemistry, cyclic voltammetry, nano-materials.

Muhammed Mizher Radhi ▪ Health and Medical Technology College-Baghdad, Middle Technology University ▪ mmradhi@yahoo.com
Yousif K. Al-Haidarie ▪ Science College, Al-mustansiriyah University
Anfal Ismael Ibrahim ▪ Science College, Al-mustansiriyah University

Érkezett: 2016. 12. 15. ▪ Received: 15. 12. 2016. ▪ http://dx.doi.org/10.14382/epitoanyag-jsbcm.2017.5

Abstract
Sodium Saccharin (NaSc) was studied as a chemical compound used for diabetic patients as a replacement for natural sugar. The study was focused on the effect of different temperatures on NaSc in human blood medium using cyclic voltammetric technique at modified glassy carbon electrode (GCE) with carbon nanotubes (CNT) as working electrode (CNT/GCE). The physical chemistry functions were studied for the activated values in terms of enthalpy (ΔH*), free energy (ΔG*) and entropy (ΔS*) for redox current peaks of NaSc in blood medium at both electrodes, GCE and CNT/GCE using Eyring equations. Also, the study included the determination of the activation energy (Ea*) determined by Arrhenius equations for the redox current peaks of NaSc to compare values obtained by GCE and CNT/GCE. It was found that the values of thermodynamic functions were different due to the oxidation – reduction reaction of NaSc in blood medium which reacts with many complex compound with the component of the blood especially hemoglobin as ferric and ferrous ions. The oxidative stress of NaSc in blood medium appeared clearly in voltammogram.
Keywords: sodium saccharin, nano-sensor, cyclic voltammetry, temperature, thermodynamic parameters.

1. Introduction

A recent study identified the extent of the impact of alternative chemical compounds for sugar such as sodium saccharin on blood composition in human blood samples, using electrochemical method [1]. Other studies used modified electrodes for the determination of chemical compounds in blood medium [2-8].

A new preparation of a biocompatible and conductive interface for immobilization and electrochemical detection of cells and application of carbon nanofiber in cyto-sensing was studied by cyclic voltammetry. The sensitivity of the method was good with a detection limit of 1×10^3 cells mL^{-1} with cells ranging from 5×10^3 to 5.0×10^7 cells mL^{-1} [9].

The redox behavior of Cd(II) and the interaction of Cd(II) with cyclic amino acid, proline, have been studied in 0.1 M KCl, 0.1 M $NaClO_4$ and acetate buffer of different pH. The CVs were recorded at glassy carbon electrode within the potential window 200 and −1500 mV. The reference and counter electrode used were Ag/AgCl and Pt wire, respectively. The cyclic voltammograms showed one pair of cathodic and anodic peaks for the Cd(II)/Cd(0) system indicating the involvement of two electron transfer processes. The peak potential shift and charge transfer rate constant (kf) values indicated the interaction between metal and ligand. The higher value of peak current ratio and peak potential separation (ΔE) indicated that the systems are quasi-reversible. The effect of supporting electrolyte and concentration of electro active species on the interaction were also studied [10].

Methionine were synthesized in aqueous electrolyte with heavy metal complexes such as Mn(II), Co(II), Ni(II), Cu(II), Zn(II), Cd(II) and Hg(II) using cyclic voltammetry. The results of the electrochemical analysis confirmed by the current potential data of peak separation (ΔE) and the peak current ratio (Ipa/Ipc) of the (Mn, Cu and Cd) complexes that the charge transfer processes are irreversible, the systems are diffusion controlled and also adsorptive controlled, and the charge transfer rate constant of metals in their complexes are less than those in their metal salts at identical experimental conditions due to the coordination of metal with methionine [11,12]. The voltammetric study of manganese complex with saccharine was studied to determine the redox current peaks of the complex as irreversible process at different pH and concentrations [13]. Linear Sweep Voltammetry and Galvanostatic Reduction techniques were used to study the oxidation of copper oxide Cu_3O_2 using vacuum and low-pressure-based to characterization the oxidation reaction [14].

In the present paper, NaSc in blood medium was studied at different high temperatures using cyclic voltammetry to determine the thermodynamic parameters of electrochemical analysis equations.

2. Experimental

2.1. Materials

Sodium saccharin (purity 98% from Chinese company), carbon nanotubes (purity 99%) supplied from Fluka company (Germany). Healthy human blood samples were received from Iraqi Blood Bank in Baghdad City of Medicine, Deionized water was used for preparation of aqueous solutions. All solutions used in the cyclic voltammetryic cell were treated with nitrogen gas for 10-15 minutes to remove the oxygen from the solutions.

2.2. Apparatus

An instrument of EZstat series (Potentiostat/Galvanostat) NuVant Systems Inc. (USA) was used in the experiments. The Electrochemical Bio-analytical cell was connected to a potentio-stat device and was monitored by a special software to perform cyclic voltammetry (CV). Silver-silver chloride reference electrode (Ag/AgCl in 3M NaCl) and Platinum wire (1 mm diameter) were used as a reference and counter electrodes, respectively. The glassy carbon working electrode (GCE) modified with CNT was used in this study after cleaning with alumina solution and treated with ultrasonic path water for ten minutes.

2.3 Preparing the modification of GCE with CNT (CNT/GCE)

Mechanical attachment technical method was employed to prepare the CNT/GCE working electrode as a nano-sensor [15,16]. The method of the modification of GCE included abrasive application of multiwall carbon nanotubes (MWCNT) on the clean surface of GCE, forming an array of MWCNT as modified working electrode MWCNT/GCE and replaced in 10 ml of electrolyte in the cyclic voltammetric cell, then connected all electrodes (working electrode, reference electrode and counter electrode) with the potentio-stat.

2.4 Measurements of different temperatures

A 10 ml size cell was used to measure the cyclic voltammograms. Solutions were replaced for studying at different temperatures. Three electrodes (working, reference and counter electrodes) as well as a thermometer were submerged into the cell to follow the solution temperature, and the three electrodes were connected to the potentio-stat. The cell was placed into a water bath to set the required temperature and a hot plate was used to increase the temperature in the cyclic voltammetic tests.

2.5 Scanning electron microscopy (SEM) study

The SEM photographs were recorded at a magnification of 1000-6000× depending on the composition of the sample. SEM analysis was carried out to investigate microcrystals. Samples were dehydrated for 45 min before being coated with gold particles using a SEM coating unit. SEM was used to examine the morphology of CNT by mechanical attached technique on a graphite electrode surface before and after electrolysis with NaSc by cyclic voltammetry using blood medium as an electrolyte. *Fig. 1.a* indicates the SEM image of CNT attached onto basal plane graphite electrode for electrolysis in blood medium that exhibited an array of microcrystals with 0.1-2 μm diameter. *Fig. 1.b* indicates the SEM image of the modified electrode after electrolysis with NaSc using cyclic voltammetry with slightly enlarged size range of 0.1-3 μm diameter indicating presence of solid to solid conversion and that the film appears stable even after 10 potential cycling.

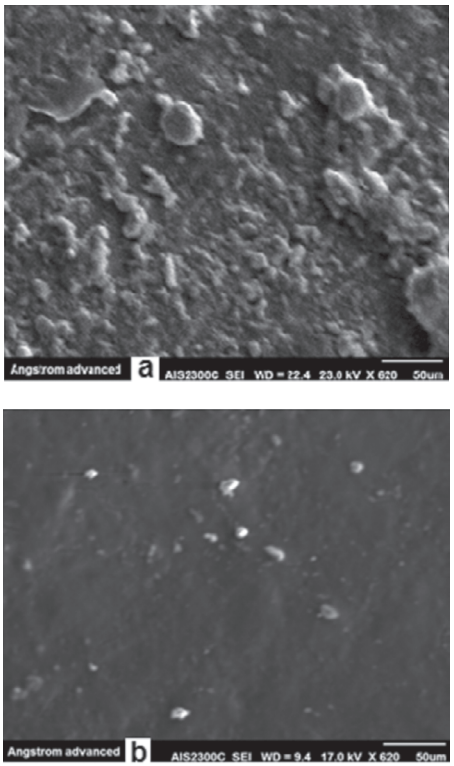

Fig. 1. Scanning Electron Microscopy (SEM): (a) of CNT attached by mechanical method onto basal plane graphite electrode after electrolysis in blood medium. (b) SEM of CNT after electrolysis of NaSc in blood medium by cyclic voltammetry.

1. ábra Pásztázó elektronmikroszkópos (SEM) felvételek: (a) a mechanikai eljárással rögzített szén nanocsövek képe a grafit elektródán vér közegben végzett elektrolízist követően. (b) a szén nanocsövek képe nátrium szacharinát elektrolízisét követően vér közegben, ciklikus voltammetriával.

3. Results and discussion

3.1. Effect of varying temperature

NaSc in blood medium was studied at different temperatures using each of GCE and modified GCE with CNT using cyclic voltammetric technique to determine the physical chemistry properties in terms of activation energy and thermodynamic parameters using Arrhenius equations [17-19] and Eyring equations [20-22], respectively.

3.1.1 Activation energy (E^*_a)

NaSc in blood medium was studied at different temperatures using GCE and CNT/GCE to determine the activation energy (E^*_a). It was found that the cathodic current peak was enhanced

gradually at the range of temperature from 29 to 40°C. *Figs 2* and *3* show the plot of Ln(I_{pc}) of NaSc versus reciprocal of temperature on GCE and CNT/GCE respectively, which is found to be fairly linear in agreement with thermodynamic expectation of Arrhenius equation; see Eqs (1) and (2) [17-19]. Also, the results of anodic current peaks are represented in *Figs 4* and *5*, illustrating the relationship between Ln(I_{pc}) of NaSc and reciprocal of temperature at GCE and modified working electrode CNT/GCE. The activation energy (E^*_a) values were calculated from the following Arrhenius equations:

$$\sigma = \sigma^\circ e^{-Ea/RT} \quad (1)$$

$$D = D^\circ e^{-Ea/RT} \quad (2)$$

Where

σ /D – conductivity/diffusibility.

σ°/ D – standard conductivity/initial diffusibility.

E_a – activation energy

R – universal gas constant

T – temperature

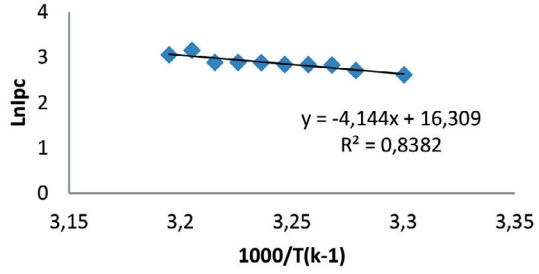

Fig. 2. Plot of Ln(I_{pc}) reduction current peak of NaSc in blood medium against inverse temperature at GCE versus Ag/AgCl as reference electrode.
2. ábra Redukciós áram csúcs Ln(I_{pc}) a hőmérséklet inverzének függvényében: nátrium szacharinát vér közegben GCE elektródával mérve (Ag/AgCl referencia elektróda mellett).

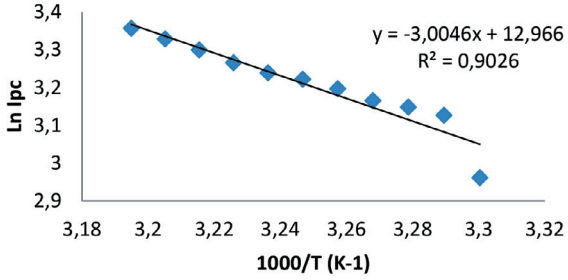

Fig. 3. Plot of Ln(I_{pc}) reduction current peak of NaSc in blood medium against inverse temperature at CNT/GCE versus Ag/AgCl as reference electrode.
3. ábra Redukciós áram csúcs Ln(I_{pc}) a hőmérséklet inverzének függvényében: nátrium szacharinát vér közegben CNT/GCE kompozit elektródával mérve (Ag/AgCl referencia elektróda mellett).

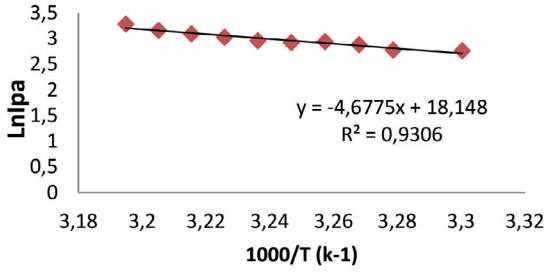

Fig. 4. Plot of Ln(I_{pa}) oxidation current peak of NaSc in blood medium against inverse temperature at GCE versus Ag/AgCl as reference electrode.
4. ábra Oxidációs áram csúcs Ln(I_{pa}) a hőmérséklet inverzének függvényében: nátrium szacharinát vér közegben GCE elektródával mérve (Ag/AgCl referencia elektróda mellett).

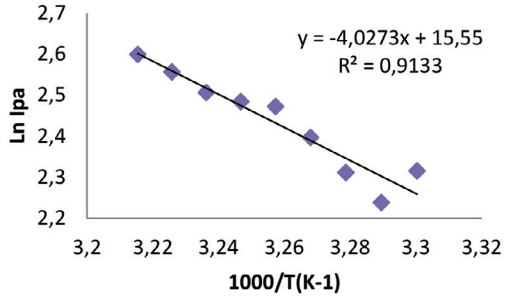

Fig. 5. Plot of Ln(I_{pa}) oxidation current peak of NaSc in blood medium against inverse temperature at CNT/GCE versus Ag/AgCl as reference electrode.
5. ábra Oxidációs áram csúcs Ln(I_{pa}) a hőmérséklet inverzének függvényében: nátrium szacharinát vér közegben CNT/GCE kompozit elektródával mérve (Ag/AgCl referencia elektróda mellett).

Fig. 6 illustrates the cyclic voltammogram of NaSc in blood medium using modified electrode CNT/GCE at 30 and 40 °C. It shows that increasing the temperature results enhancement of both the oxidation-reduction current peaks of NaSc. Moreover, the nano-sensor results improvement of the current as an electro-catalyst in blood medium.

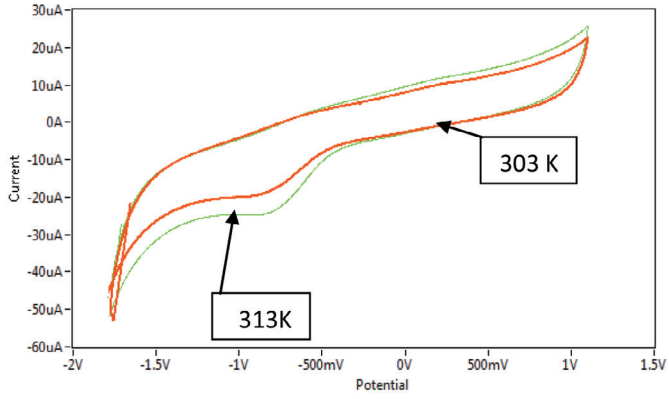

Fig. 6. Cyclic voltammogram of NaSc in blood medium at 303K and 313K at CNT/GCE.
6. ábra Nátrium szacharinát ciklikus voltammogramja vér közegben, 303K és 313K hőmérsékleten, CNT/GCE kompozit elektródával mérve.

The values of activation energy of cathodic (E^*a_{pc}) and anodic (E^*a_{pa}) current peaks of NaSc in blood medium at CNT/GCE are 24.98 kJ/mol.K and 33.48 kJ/mol.K respectively that can be compared with the values at GCE which is E^*a_{pc} = 34.45 kJ/mol.K and E^*a_{pa} = 25.96 kJ/mol.K as shown in Table 1. By comparing the activation energy values of NaSc in blood medium at GCE and CNT/GCE, it can be concluded that the value of E^*a_{pc} was declined from 34.45 at GCE to 24.98 because of using the nano-sensor of working electrode. But, in oxidation process of NaSc in blood medium the activation energy at GCE is less than that of at modified electrode CNT/GCE. It can be attributed to the viscosity of blood components which act as inhibition of the anodic conductivity [22].

3.1.2 Thermodynamic functions

Activation free energy (G^*), enthalpy (H^*) and entropy (S^*) of NaSc in blood medium at CNT/GCE and GCE were determined from Erying equation, see Eq. (3) [20-22] and thermodynamic equations [23]:

$\Delta G^* = -RT \text{ Ln } (k\ h / T\ k_B)$ (3)

$\Delta H^* = \Delta G^* + T\ \Delta S^*$ (4)

And $\Delta H^* = \Delta G^* + T\ \Delta S^*$ (5)

The different units are accounted for in using either the gas constant R (8.314 $J.mol^{-1}k^{-1}$), the Boltzmann constant k_B (1.381×10^{-23} $m^2kg.sec^{-2}k^{-1}$), and Planck constant h (6.66×10^{-34} J.sec) as the multiplier of temperature T (K).

Table 1 illustrates the thermodynamic functions of NaSc in blood medium, the results in the table can be concluded that the spontaneous reaction was depended on more than one factors according to the law of Gibbs free energy, not only depend on change in enthalpy (ΔH*) to interact and build on the Gibbs law, the reaction is becoming spontaneous when the free energy change)ΔG*) is negative and enthalpy change (ΔH*) is also negative, but entropy (ΔS*) is positive [23]. The electrochemistry reactions such as the oxidation – reduction process for NaSc compound in blood medium was studied at different temperatures to find out if the status of the reaction for the oxidation-reduction is spontaneous or nonspontaneous. Also, the working electrode affected the processes as electro-catalyst for enhancement the current in the system when using nanoparticles like CNT. In this study, the modified working electrode CNT/GCE was used to determine the functions as shown in *Table 1* to study the reduction and oxidation current peaks of NaSc in blood medium which were indicated in *Figs 2-5*.

Reaction status	Ea*	ΔS*	ΔH*	ΔG*	Electrode	Type of Reaction
nonspontaneous reaction	+34.453	-70.782	-2.529	+68.253	GCE	reduction
nonspontaneous reaction	+24.980	+0.218	+2.536	+67.294	CNT/GCE	reduction
nonspontaneous reaction	+32.021	-2.286	-2.529	+67.975	GCE	oxidation
nonspontaneous reaction	+33.483	-0.124	+30.92	+69.176	CNT/GCE	oxidation

Table 1 Activation energy and thermodynamic functions of NaSc in blood media at GCE and CNT/GCE.

1. táblázat Aktiválási energia és termodinamikai paraméterek; nátrium szacharinát vér közegben GCE és kompozit CNT/GCE elektródával mérve.

4. Conclusions

The effect of different working temperature on redox process of NaSc in blood medium was studied at different electrodes (GCE and CNT/GCE) in cyclic voltammetric method to determine the thermodynamic functions and activation energy using Arrhenius equations and Eyring equation. Sodium saccharine has oxidation–reduction current peaks in blood medium, so it can be considered that NaSc is an oxidative reagent in blood medium with the oxidation current peak at 750 mV. Activation energy values were determined from Arrhenius equations at both GCE and CNT/GCE electrodes for both cathodic and anodic peaks; nanoparticles made activation energy values to be reduced in blood medium. Activation of free energy (G^*), enthalpy (H^*) and entropy (S^*) of NaSc in blood medium can be calculated from Eyring equation and other thermodynamic equations. The same values were found for each electrodes (GCE and CNT/GCE), so the values of thermodynamic functions are not effected by the electrode, but the spontaneous oxidation-reduction reaction depended on these functions.

References

[1] Takayama, S. – Sieber, S. M. – Adamson, R. H. – Thorgeirsson, U. P. – Dalgard, D. W. – Arnold, L. L. – Cano, M. – Eklund, S. – Cohen, S. M. (1998): Long-term feeding of sodium saccharin to nonhuman primates: implications for urinary tract cancer. *Journal of the National Cancer Institute*, Vol. 90, No. 1, pp. 19–25. https://doi.org/10.1093/jnci/90.1.19

[2] Radhi, M. M. – Abdullah, H. N. – Al-Asadi, S. A. – Al-Mulla, E. A. J. (2015): Electrochemical oxidation effect of ascorbic acid on mercury ions in blood sample using cyclic voltammetry, *International Journal of Industrial Chemistry*, Vol. 6, pp. 311–316. https://doi.org/10.1007/s40090-015-0053-9

[3] Radhi, M. M. – Albakry, A. A. A. – Jassim, A. M. – Alassady, S. A. – Al-Mulla, E. A. J. (2016): Electrochemical Study of Pb(II) in Present of Each Ascorbic Acid, Glucose, Urea and Uric Acid Using Blood Medium as an Electrolyte, *Nano Biomedicine and Engineering*, Vol. 8, No. 1, pp. 9-15. https://doi.org/10.5101/nbe.v8i1.p9-15.

[4] Radhi, M. M. – Khalaf, M. S. – Ali, Z.O. – Omran, R. I. (2016): Voltammetric Analysis of Zn (II) in Present of Each Ascorbic Acid (AA) and Folic Acid (FA) in Human Blood Samples, American Association for Science and Technology, *AASCIT Communications*, Vol. 3, No. 1, pp. 11-16.

[5] Radhi, M. M. – Abdul-Amir, Y. K. – Khalaf, M. S. (2016): Electrochemical Effect of Acetylsalicylic Acid (Aspirin) in Present of Each Ascorbic Acid (AA) and Folic Acid (FA) in Normal Saline and Human Blood Samples, American Association for Science and Technology *AASCIT Communications*, Vol. 3, No. 3, pp. 152-159.

[6] Radhi, M. M. – Al-Dulimy, W. G. – Khalaf, M. S. (2016): Electrochemical study of selenium (IV) mediated by carbon nanotubes modified glassy carbon electrode in blood medium, *Építőanyag-Journal of Silicate Based and Composite Materials*, Vol. 68, No. 3, pp. 90-93. https://doi.org/10.14382/epitoanyag-jsbcm.2016.16

[7] Banan, D. – Tan, W. T. – Sulaiman, Y. – Yusri, M. F. – Zidan, M. – Ab Ghani, S. (2013): Electrochemical Oxidation of Ascorbic Acid Using MgB2- MWCNT Modified Glassy Carbon Electrode, *International Journal of Electrochemical Science*, Vol. 8, pp. 12519 – 12530.

[8] Perenlei, G. – Tee, T. W. – Yusof, N. A. – Kheng, G. J. (2011): Voltammetric Detection of Potassium Ferricyanide Mediated by Multi-walled Carbon Nanotube/Titanium Dioxide Composite Modified Glassy Carbon Electrode, *International Journal of Electrochemical Science*, Vol. 6, pp. 520 – 531.

[9] Hao, C. – Ding, L. – Zhang, X. – Ju, H. (2007): Biocompatible Conductive Architecture of Carbon Nanofiber-Doped Chitosan Prepared with Controllable Electrodeposition for Cytosensing, *Analytical Chemistry*, Vol. 79, No. 12, pp, 4442–4447. https://doi.org/10.1021/ac062344z

[10] Hasan, M. – Hossain, E. – Mamun, M. A. – Ehsan, M. Q. (2012): Study of redox behavior of Cd(II) and interaction of Cd(II) with proline in the aqueous medium using cyclic voltammetry, *Journal of Saudi Chemical Society*, Vol. 16, No. 2, pp. 145–151. https://doi.org/10.1016/j.jscs.2011.06.006

[11] Mamun, M. A. – Ahmed, O. – Bakshi, P. K. – Ehsan, M. Q. (2010): Synthesis and spectroscopic, magnetic and cyclic voltammetric characterization of some metal complexes of methionine: [(C 5H 10NO 2S) 2M II]; M II = Mn(II), Co(II), Ni(II), Cu(II), Zn(II), Cd(II) and Hg(II), *Journal of Saudi Chemical Society*, Vol. 14, No. 1, pp. 23-31. https://doi.org/10.1016/j.jscs.2009.12.005

[12] Johns, C. A. – Hossain, G. M. G. – Malik, K. M. A. (2001): Structural studies of Ni(II), Zn(II) and Cd(II) complexes with saccharinate and 2,2´-bipyridine ligands, *Polyhedron*, Vol. 20, No. 7-8,pp. 721-726. http://doi.org/10.1016/S0277-5387(01)00702-1

[13] Islam, G. J. – Akhtar, H. M. N. – Mamun, M. A. – Ehsan, M. Q. (2009): Investigations on the redox behaviour of manganese in manganese(II)–saccharin and manganese(II)–saccharin–1,10-phenanthroline complexes, *Journal of Saudi Chemical Society,* Vol. 13, No. 2, pp. 177-183. https://doi.org/10.1016/j.jscs.2009.05.002

[14] Cocke, D. L. – Schennach, R. – Hossain, M. A. – Mollah, M. Y. A. (2005): The low-temperature thermal oxidation of copper, Cu3O2, and its influence on past and future studies, *Vacuum*, Vol. 79, pp. 71–83. https://doi.org/10.1016/j.vacuum.2005.01.010

[15] Scholz, F. – Lange, B. (1992): Abrasive stripping voltammetry - an electrochemical solid state spectroscopy of wide applicability, *TrAC Trends in Analytical Chemistry*, Vol. 11, pp. 359-367. https://doi.org/10.1016/0165-9936(92)80025-2

[16] Tan, W. T. – Ng, G. K. – Bond, A. M. (2000): Electrochemical of microcrystalline tetrathiafulvalene at an electrode solid aqueous KBr interface, *Malaysian Journal of Chemistry*, Vol. 2, pp. 34-42.

[17] Tan, W. T. – Lim, E. – Bond, A. (2003): Voltammetric studies on microcrystalline C_{60} adhered to an electrode surface by solvent casting and mechanical transfer methods. *Journal of Solid State Electrochemistry*, Vol. 7, pp. 134-140. https://doi.org/10.1007/s10008-002-0295-2

[18] Tan, W. T. – Goh, J. (2008): Electrochemical oxidation of methionine mediated by a fullerene-C_{60} modified gold electrode. *Electroanalysis*, Vol. 20, pp. 2447–2453. https://doi.org/10.1002/elan.200704335

[19] Jacob, S. – Hong, Q. – Coles, B. – Compton, R. (1999): Variable-Temperature Microelectrode Voltammetry: Application to Diffusion Coefficients and Electrode Reaction Mechanisms. *Journal of Physical Chemistry B*, Vol. 103, pp. 2963-2969. https://doi.org/10.1021/jp990024w

[20] Evans, M. G. – Polanyi, M. (1935): Some applications of the transition state method to the calculation of reaction velocities, especially in solution. *Transactions of the Faraday Society,* Vol. 31, pp. 875–894. https://doi.org/10.1039/TF9353100875

[21] Polanyi, J. C. (1987): Some concepts in reaction dynamics. *Science*, Vol. 236, pp. 680–690. https://doi.org/10.1126/science.236.4802.680

[22] Chapman, S. – Cowling, T. G. (1991): The Mathematical Theory of Non-uniform Gases: An Account of the Kinetic Theory of Viscosity, Thermal Conduction and Diffusion in Gases (3rd Edition). *Cambridge University Press*, 1991

[23] Daniels, F. – Alberty, R. A. (1984): Physical Chemistry, *John Wiley & Sons Inc*; 6th edition (May 1984).

Ref.:
Radhi, Muhammed Mizher – **Al-Haidarie,** Yousif K. – **Ibrahim,** Anfal Ismael: *The electrochemical effect of different temperatures on sodium saccharine in blood medium using modified working electrode CNT/GCE by cyclic voltammetry*
Építőanyag – Journal of Silicate Based and Composite Materials, Vol. 69, No. 1 (2017), 24–28. p.
http://dx.doi.org/10.14382/epitoanyag-jsbcm.2017.5

A hőmérséklet elektrokémiai hatása nátrium szacharinátra vér közegben ciklikus voltammetriai vizsgálatok során CNT/GCE elektródával mérve

A cikk bemutatja a hőmérséklet hatását nátrium szacharinátra emberi vér közegben ciklikus voltammetriai vizsgálatok során. A méréseket szén nanocsövekkel (CNT) módosított üvegszerű szén elektródával (GCE) végezték. A fizikai kémiai paramétereket (entalpia, szabad energia és entrópia) az Eyring egyenletekből határozták meg mindkét elektróda típus (GCE és CNT/GCE) esetén a redox áramcsúcsok mérési eredményei alapján. Az aktiválási energia mértékét az Arrhenius egyenletekből határozták meg a redox áramcsúcsok mérési eredményei alapján. A vizsgálatok rámutattak, hogy a termodinamikai paraméterek eltérőek a nátrium szacharinát oxidációs-redukciós reakciói következtében, elsősorban a vér vasion tartalmú hemoglobinjával.
Kulcsszavak: nátrium szacharinát, nano-szenzor, ciklikus voltammetria, hőmérséklet, termodinamikai paraméterek.

Thermodynamic parameters of mixtures with allowance for phase transition components under shock-wave loading

Sergey A. Kinelovskii
Doctor of Sciences, full Professor, chief scientist in LIH SB RAS. Author and co-author of more than 100 papers that includes WoS and Scopus publications.

Konstantin K. Maevskii
Scientist in LIH SB RAS. Scientific degree Candidate of Physico-mathematical Sciences 2011. Topic of PhD work "The model of dynamic loading of heterogeneous porous materials". Assistant professor at the SIBSTRIN. Author or co- author of more than 30 articles.

Sergey A. KINELOVSKII ▪ Lavrent'ev Institute of Hydrodynamics, Siberian Branch, Russian Academy of Sciences ▪ skin@hydro.nsc.ru
Konstantin K. MAEVSKII ▪ Lavrent'ev Institute of Hydrodynamics, Siberian Branch, Russian Academy of Sciences

Érkezett: 2016. 12. 16. ▪ Received: 16. 12. 2016. ▪ http://dx.doi.org/10.14382/epitoanyag-jsbcm.2017.6

Abstract
The shock-wave synthesis and compaction using powder mixtures are the one of perspective directions of new materials creation. The results of numerical experiments on modeling of shock wave loading of mixtures with allowance for phase transition components in their composition are presented. The significant change in volume in the region of phase transition components included in the mixtures allows us to expand the range of variation of thermodynamic parameters of the mixtures under shock wave loading. The calculation model is based on the assumption that all components of mixture under shock-wave loading are in thermodynamic equilibrium (model TEC). The model TEC allows us to describe the region of the polymorphic phase transition, considering the material in the region of phase transition as a mixture of low-pressure phase and high-pressure phase. The good agreement of these model calculations with the data of different authors defined on the basis of experiments is obtained. Thermodynamic parameters of the nitrides mixture, solid and porous mixtures with quartz as component were reliably described. This model is useful for determining the compositions and volume fractions of the components of the mixture to obtain the specified parameters of solid and porous materials under shock-wave loading.
Keywords: High pressure engineering, Integrated circuits, Mixtures, Phase transitions, Porous materials, Shock waves, Thermodynamic equilibria

1. Introduction

The possibility of changes in the structure and phase composition of mixtures under the action of

shock waves is of interest for the creation of materials with the desired properties. Materials experiencing a phase transition under shock wave loading are of particular interest when solving this task. On one hand, such materials, e.g., quartz, graphite, bismuth and others have a high compression ratio that allows you to expand the field of the feasible thermodynamic parameters [1, 2]. This gives the opportunity to purposefully achieve the conditions necessary for the production of ceramics with the given properties. On the other hand, many materials with unique properties are also experiencing a phase transition, which further stimulates interest in such research. There are different methods for modeling the thermodynamic parameters of shock-wave loading of mixtures [3], which, however, does not describe the data obtained on the basis of the experiment in the whole range of parameters, in contrast to the model TEC [4].

The interest in the research of compressibility of quartz mixtures is related to the properties of quartz and the possibility of creating materials with the required properties (heat-resistant and high- strength ceramics). The wide distribution of quartz in nature has led to much attention to it. The mass fraction of quartz is more than 60% taking into account mix and silicates in the earth's crust; the free quartz content is 12 %. As a consequence, there is the large base of experimental data on shock-wave loading on quartz and mixture with it that allows you to check the accuracy of the simulation.

Nitrides are often refractory and resistant to stress at high temperatures substances. Nitride coatings are used in energy, space technology, imparts hardness and corrosion resistance of products. The advantage of aluminum nitride AlN over other materials is the unique combination of its physical and electrical characteristics: such as the high thermal conductivity, good insulating properties, the moderate coefficient of thermal expansion at relatively low cost. Recent interest in silicon nitride Si_3N_4 is associated with the discovery of its high-pressure modification with a cubic structure (γ-phase) which has a considerable hardness comparable to that of stishovite—the high-pressure phase of SiO_2. Some researchers believe that stishovite takes the third place in this parameter, after diamond and cubic boron nitride. This feature of the γ-phase allows considering it as a promising technological material, though very high pressures more than 15 GPa and temperatures more than 1000 K required for the formation of γ-Si_3N_4 are a major obstacle not only to industrial use, but also to a detailed study of its properties. Therefore, the selection of optimal conditions under which it would be possible to synthesize relatively large amounts of this substance with a high output at acceptable values of external parameters (pressure and temperature) is a topical task. High temperature is important along with pressure in

the formation of γ-Si_3N_4. The promising method of high-temperature shock compression is used to research phase transition in silicon nitride and achievements of γ phase [5]. This method allows increasing the substance's temperature during compression, thereby promoting the transformation, and significantly reducing the residual temperature after the pressure drop, thereby ensuring quenching of the new phase. The effect is achieved by addition of components with high compressibility and specific heat, such as alkali halide salts, to the samples.

The model TEC that used in this work can reliably describe the thermodynamic parameters of the mixture under shock wave loading, including the region of phase transition of components. It should be noted, that the model TEC uses the parameters of the equation of state of the components and hence allows considering the interaction of mixture components, unlike the mixed method, which is mainly used for high-density mixtures [5].

2. Calculation model

The model TEC is used to describe the thermodynamic parameters of porous solids and mixtures of powders under shock wave loading [1, 4]. The equation of state of the Mie–Grüneisen type is applied when modeling the thermodynamic parameters of condensed phases. The initial internal energy and pressure of the substances are zero under normal conditions, taking into account the fact, that field of use of this model for pressures is over 5 GPa. Hence, the equation of state for condensed component has the form with the current and initial densities ρ and ρ_0, pressure P, specific heat c_v, and the current and initial temperatures T and T_0:

$$P(\rho,T) = A\left[\left(\rho/\rho_0\right)^k - 1\right] + \Gamma(T)c_v(T-T_0)\rho \qquad (1)$$

The function Γ(T) has the following form:

$$\Gamma(T) = \left\{\left[\Gamma(T_0)-\Gamma(T_\infty)\right]^{-1} + C(T-T_0)\right\}^{-1} + \Gamma(T_\infty) \qquad (2)$$

$$C = \left\{\left[\Gamma(T_*)-\Gamma_\infty)\right]^{-1} - \left[\Gamma(T_0)-\Gamma_\infty\right]^{-1}\right\}(T_*-T_0)^{-1} \qquad (3)$$

The parameters C, $\Gamma(T_\infty)$ are chosen from the condition of compliance of the calculated shock adiabats with known experimental results for every component, so that:

$\Gamma(T) \to \Gamma(T_0)$ when $T \to T_0$,
$\Gamma(T) \to \Gamma(T_\infty)$ when $T \to T_\infty$.

Here value of $\Gamma(T_0)$ is taken on the basis of known data at normal conditions. The coefficient C, which allows describing the experimental points upon moderate compression, is determined by the intermediate value $\Gamma(T_*)$ at temperature $T=T_*$. The asymptotic value $\Gamma(T_\infty)$ corresponds to the maximum temperatures. For the gas, we use the equation of state of ideal gas. We write the conditions of dynamic compatibility on the shock wave front, which are laws of conservation of the mass flux for each component of the mixture and laws of conservation of momentum and energy fluxes for the mixture as a whole [1, 4]. The resultant equations combined with the equation of state for each component are sufficient to find dependences of the type of $P(U)$ or $D(U)$, which can be treated as the shock adiabats of the multicomponent mixture. U and D are the mass and wave velocity, respectively. A, k, and Γ are the coefficients in the equations of state of the condensed component. For the mixture of n condensed components with the initial volume fraction μ_{n0} we can obtain the expression:

$$P = \left\{\sum_{i=1}^{n} A_i \frac{\mu_{i0}}{\sigma_i}\left[\left(h_i - \frac{k_i+1}{k_i-1}\right)\sigma_i^{n_i} + \frac{2k_i\sigma_i}{k_i-1} - h_i - 1\right]\right\}$$
$$\left[\sum_{i=1}^{n}\frac{\mu_{i0}}{\sigma_i}h_i + \left(\frac{h_g}{\sigma_g}\right)\left(1-\sum_{i=1}^{n}\mu_{i0}\right) - 1\right]^{-1} \qquad (4)$$

Here $h_i = 2/\Gamma_i + 1$, $i = 1\ldots n$, $h_g = 2/(\gamma-1)+1$. $\sigma_i = \rho_i/\rho_{i0}$, $\sigma_g = \rho_g/\rho_{g0}$ is the compression ratio of components, ρ_g, ρ_{g0} current and initial gas densities, $\gamma = 1.41$ is the ratio of specific heat. In view of equal temperatures of all components, including gas, we finally have an $n + 1$ equation for $n + 2$ variables P, σ_i (i=1…n), σ_g, which allows us to construct a shock adiabat of mixture. A pure substance is considered as a mixture with one condensed component. The volume fraction of gas is assumed zero for calculation of parameters of solid material.

The model TEC may describe the behavior of the materials including the phase transition region. The material is considered as the mixture of low-pressure phase and high-pressure phase in this area. We write the conditions of dynamic compatibility on the shock wave front taking into account the phase transition. It is assumed that the volume fraction α of low-pressure phase passed into high- pressure phase in the region of polymorphic phase transition. The dependence of low-pressure phase, turning into the high-pressure phase, we can specify the following expression $\alpha = k\Delta E$ in the first approximation in the phase transition region. Here $k = (E_f - E_b)^{-1}$, E_b is internal energy at the beginning of the phase transition, E is current internal energy, $\Delta E = E_f - E_b$, E_f is internal energy at the finish of the phase transition, when there are full transition of low-pressure phase to high-pressure phase. The comparison of the calculations with the experimental data has shown that the value of k, defined for one of the porosity, allows one to describe the results for other values of the porosity. As the result, the three regions are set depending on the value of α that determines the volume of low-pressure phase and high-pressure phase of the shock adiabats for the materials with the phase transition [6]:

$$\begin{cases} E \le E_0 & \alpha = 0 \\ E_0 \le E \le E_k & \alpha = k\Delta E \\ E \ge E_k & \alpha = 1 \end{cases}$$

3. Numerical results

The accuracy of the modeling materials used to create materials with desired properties, with the components experiencing a phase transition under shock wave loading, is confirmed, in particular, calculations of the shock adiabats for mixtures of quartz. Calculations of thermodynamic

parameters of the mixtures of quartz with aluminum mass fractions wt. % Al (30) SiO_2 (70), Al (40) SiO_2 (60), Al (50) SiO_2 (50) are shown in *Fig.* 1. The calculation for pure quartz is given on the same figure for illustration. The possibility of accounting for the phase transition during shock-wave loading for the first time allows us to describe all the data obtained on the basis of experiments for all the considered mixtures.

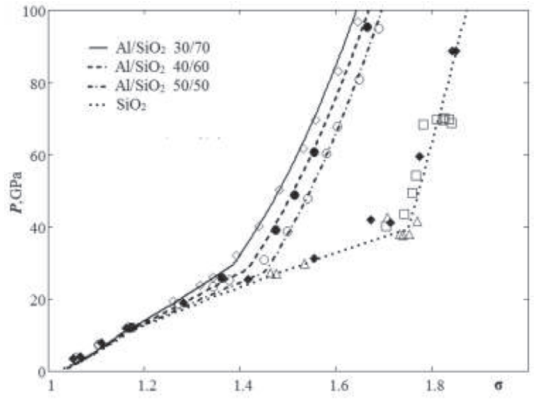

Fig. 1. Shock adiabats in coordinates pressure – compression. The calculation and experimental results for the mixtures of quartz with aluminum of various compositions, and pure quartz. Experimental data from [7].

1. ábra Lökéshullám adiabata vonalak nyomás-kompresszió koordináta rendszerben. Számított és kísérleti eredmények eltérő összetételű kvarc-alumínium keverékekre és tiszta kvarcra vonatkozóan. A kísérleti eredmények forrása [7].

The model TEC allows describing the shock adiabats in the region of the phase transition of quartz mixtures with the significantly different components, in particular by density. Calculations of the mixtures of quartz with tungsten and quartz with teflon, as well as data obtained on the basis of the experiments [7] are shown in *Fig.* 2. The calculations were performed for the mixtures of following compositions: mixture of quartz with tungsten (density 10.19 g/cm^3), weight fraction wt.% W(88) SiO2 (12) and mixture of quartz with teflon wt.% SiO2 (55) Teflon (45), (density 2.38 g/cm^3). The calculations allow describing the data obtained on the basis of experiments with good accuracy.

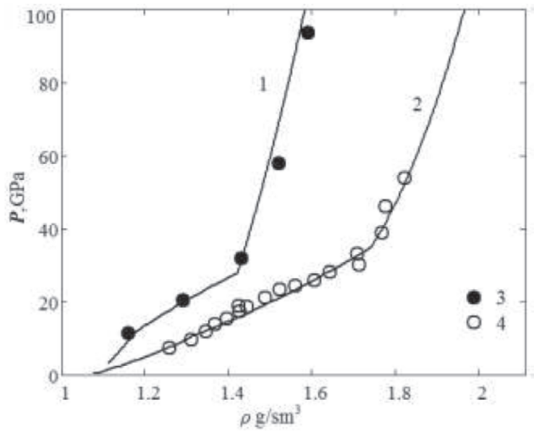

Fig. 2. Shock adiabats of mixture of quartz with tungsten (1), mixture of quartz with teflon (2). Experimental data (3), (4) from [7].

2. ábra Lökéshullám adiabata vonalak kvarc-volfrám keverékre (1), kvarc-teflon keverékre (2). A kísérleti eredmények (3), (4) forrása [7].

The model parameters allowing reliable description of the thermodynamic parameters of pure nitrides under shock wave loading are used to simulate the parameters of the mixture of nitrides as components [6].

The experimental data [8] for aluminum nitride AlN (initial density 3.23 g/cm^3) and the data [9] for silicon nitride Si_3N_4 (initial density 3.44 g/cm^3) are used in the calculations of the shock wave loading of these materials with the phase transition. The shock adiabats are shown in *Fig.* 3.a with the shift for clarity. The initial pressures of the phase transition for AlN and for Si_3N_4 are prescribed at 20 and 30 GPa respectively. The transition of β-phase into highly-dense *c*-phase is reproduced in the calculations for Si_3N_4. The first three experimental points respective to the *a*-phase (corresponding to plastic deformation) did not take into account as it was done in [9]. The calculations show that the model TEC allows one to describe the unusual behavior of the shock adiabats [8] in the phase transition region (reduction of wave velocity with increasing of mass velocity).

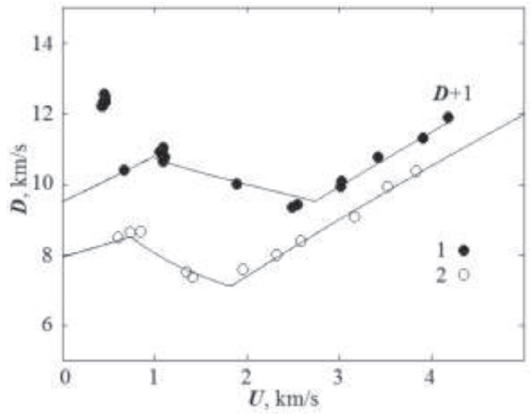

(a)

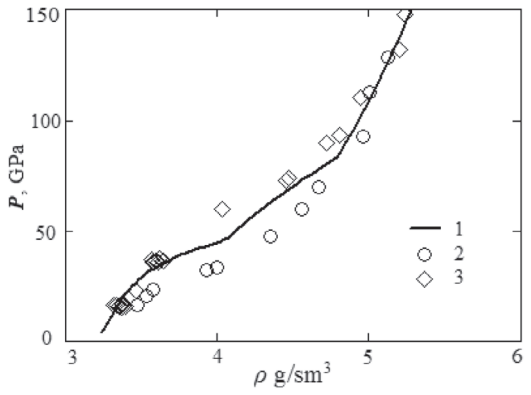

(b)

Fig. 3. Shock adiabats of silicon nitride (1) and nitride of aluminum (2) in the coordinates of wave and mass velocity (a). Shock adiabats of the mixture AlN and Si3N4 (1), experimental data of silicon nitride (2) [9] and aluminum nitride (3) [8] in the coordinates pressure and density (b).

3. ábra Lökéshullám adiabata vonalak szilícium-nitridre (1), alumínium-nitridre (2) lökéshullám sebesség és impulzus koordináta rendszerben (a). Lökéshullám adiabata vonalak AlN - Si3N4 keverékre (1), kísérleti eredmények szilícium-nitridre (2) [9] és alumínium-nitridre (3) [8] vonatkozóan, nyomás-sűrűség koordináta rendszerben (b).

The results for the mixture of AlN and Si_3N_4 with equal volume fractions and initial density 3.335 g/cm^3 are shown in *Fig.* 3.b. Here the experimental data for pure AlN and

Si3N4 [8, 9] are shown for the comparison. The beginning of the phase transition for AlN and Si_3N_4 in the mixture are determined at the same pressure as that for pure substances.

The calculations for the mixtures of oxides are also performed on account of a large interest in silicon nitride and its compounds. Thermodynamic parameters are simulated for mixtures of Si_3N_4 with oxide, which were obtained on the basis of the experiments data [10]. The calculation for the mixture of Si_3N_4 and periclase MgO is shown in *Fig.* 4. MgO is used in industry for the production of refractories, including very fine abrasives for cleaning surfaces, in particular in electronics. The simulated mixture is characterized by the weight fraction wt % Si_3N_4 (95) MgO (5) and the density 3.164 g/cm^3

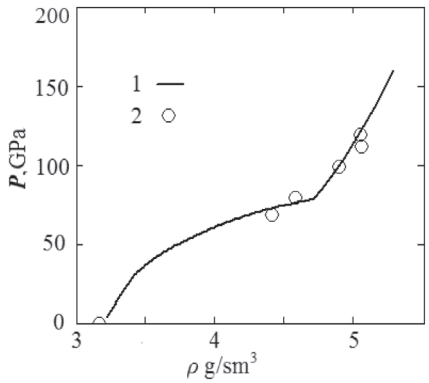

Fig. 4. Calculation for the mixture of Si_3N_4 and MgO with the phase transition (1). Experimental data (2) [10].

4. ábra Számított eredmények Si_3N_4 - MgO keverékre, fázisátalakulással (1). Kísérleti eredmények (2) forrása [10].

The results show the accuracy of the description of thermodynamic parameters of the mixtures of this type under shock wave loading. The prospects of using materials with phase transition are shown taking into account their unique properties and possibility to change the values of pressure and temperature of mixtures in a wider range of values. This approach extends the range of achievable values of thermodynamic parameters.

4. Conclusions

The data of the model TEC calculations correspond well to the experimental data by various authors. The model parameters allow us to reliably describe the behavior of pure materials under shock wave loading were used to simulate thermodynamic parameters of mixtures with components experiencing a phase transition under shock wave loading. It was shown that the TEC model allows us to simulate thermodynamic parameters of mixtures under shock wave loading including mixtures that contain components experiencing phase transitions. The simulation results allow determining the ratio of mixture components with the aim of obtaining specified parameters of solid and porous materials after their exposure to shock waves for the synthesis of ceramics with desired properties.

References

[1] S. A. Kinelovskii, – Maevskii, K. K. (2016): Estimation of the thermodynamic parameters of a shock-wave action on high-porosity heterogeneous materials. *Technical Physics*, Vol. 61,No. 8, pp. 1244-1249. https://doi.org/10.1134/S1063784216080144

[2] Kinelovskii, S. A. – Maevskii, K. K. (2016): Modeling shock loading of multicomponent materials including bismuth. *High Temperature*, Vol. 54, No. 5, pp. 675-681. https://doi.org/10.1134/S0018151X16050163

[3] Oren, E. P. –Francois, X. (2010): Comparison of methods for calculating the shock hugoniot of mixtures. *Shock Waves*, Vol. 20, No. 1, pp. 73-83. https://doi.org/10.1007/s00193-009-0230-x

[4] Kinelovskii, S. A. – Maevskii, K. K. (2013): Model of the behavior of the mixture with different properties of the species under high dynamic loads. *Journal of Applied Mechanics and Technical Physics*, Vol. 54, No. 4, pp. 524-530. https://doi.org/10.1134/S0021894413040020

[5] Yakushev, V. V. – Zhukov, A. N. – Utkin, A. V. – Rogacheva, A. I. – Kudakina, V. A. (2015): Formation of cubic silicon nitride from the low-pressure phase by high-temperature shock compression. *Combustion, Explosion and Shock Waves*, Vol. 51, No. 5, pp. 603-610. https://doi.org/10.1134/S0010508215050123

[6] Maevskii, K. K. – Kinelovskii, S. A. (2014): Model of behavior of nitrides and their mixtures under high dynamic loads. *AIP Conf. Proc.*, Vol. 1623, International conference on physical mesomechanics of multilevel systems, 3–5 September 2014, p. 391. https://doi.org/10.1063/1.4898964

[7] Levashov, P. R. – Khishchenko, K. V. – Lomonosov, I. V. – Fortov, V. E. (2004): Database on Shock-Wave Experiments and Equations of State Available via Internet. *AIP Conf. Proc.*, Vol. 706, Proceedings of the Conference of the American Physical Society Topical Group on Shock Compression of Condensed Matter, 20-25 July 2003, pp. 87-90. https://doi.org/10.1063/1.1780190

[8] Bakanova, A. A. – Bugaeva, V. A. – Dudoladov, I. P. – Trunin, R. F. (1995): Fizika Zemli, Vol. 6

[9] He, H. – Sekine, T. – Kobayashi, T. – Hirosaki, H. (2000): Shock-induced phase transition of β–Si_3N_4 to c–Si_3N_4. Physical Review B, Vol. 62, No. 17, p. 11412. https://doi.org/10.1103/PhysRevB.62.11412

[10] Marsh, S. P. (1980): LASL Shock Hugoniot Data, *University of California Press*

Ref.:
Kinelovskii, S. A. – **Maevskii**, K. K.: *Thermodynamic parameters of mixtures with allowance for phase transition components under shock-wave loading*
Építőanyag – Journal of Silicate Based and Composite Materials, Vol. 69, No. 1 (2017), 29–32. p.
http://dx.doi.org/10.14382/epitoanyag-jsbcm.2017.6

Új anyagok kifejlesztésének egyik irányzata a por keverékek nagy nyomás alatti szintézise

A cikk numerikus vizsgálatok eredményeit ismerteti a lökéshullámok által gerjesztett fázisátalakulások területén. A nagymértékű térfogatváltozás a fázisátalakulások során lehetőséget teremt a termodinamikai paraméterek kibővítésére a lökéshullámok által gerjesztett jelenségeknél. Az ismertetett számítási modell alapfeltevése, hogy a keverékek összetevői a lökéshullámok alatt termodinamikai egyensúlyban vannak. A modell lehetőséget nyújt a polimorf fázisátalakulások leírására, feltételezve, hogy az anyag a fázisátalakulás során egy kis nyomású fázis és egy nagy nyomású fázis keveréke. A modell alapján számított eredmények jó egyezést mutatnak a publikált kísérleti eredményekkel. A cikk bemutat nitrid-kvarc keverékekre, tömör és porózus anyagokra vonatkozó eredményeket.
Kulcsszavak: magasnyomású mérnöki módszerek, integrált áramkör, keverék, fázisátalakulás, porózus anyagok, lökéshullám, termodinamikai egyensúly

GUIDELINE FOR AUTHORS

The manuscript must contain the followings: title; author's name, workplace, e-mail address; abstract, keywords; main text; acknowledgement (optional)**; references; figures, photos with notes; tables with notes; short biography** (information on the scientific works of the authors).

The full manuscript should not be more than 6 pages including figures, photos and tables. Settings of the word document are: 3 cm margin up and down, 2,5 cm margin left and right. Paper size: A4. Letter size 10 pt, type: Times New Roman. Lines: simple, justified.

TITLE, AUTHOR

The title of the article should be short and objective.

Under the title the name of the author(s), workplace, e-mail address.

If the text originally was a presentation or poster at a conference, it should be marked.

ABSTRACT, KEYWORDS

The abstract is a short summary of the manuscript, about a half page size. The author should give keywords to the text, which are the most important elements of the article.

MAIN TEXT

Contains: materials and experimental procedure (or something similar), results and discussion (or something similar), conclusions.

REFERENCES

References are marked with numbers, e.g. [6], and a bibliography is made by the reference's order. References should be provided together with the DOI if available.

Examples:

Journals:

[6] Mohamed, K. R. – El-Rashidy, Z. M. – Salama, A. A.: In vitro properties of nano-hydroxyapatite/chitosan biocomposites. *Ceramics International.* 37(8), December 2011, pp. 3265–3271, http://dx.doi.org/10.1016/j.ceramint.2011.05.121

Books:

[6] Mehta, P. K. – Monteiro, P. J. M.: Concrete. Microstructure, properties, and materials. *McGraw-Hill*, 2006, 659 p.

FIGURES, TABLES

All drawings, diagrams and photos are figures. The **text should contain references to all figures and tables**. This shows the place of the figure in the text. Please send all the figures in attached files, and not as a part of the text. **All figures and tables should have a title**.

Authors are asked to submit color figures by submission. Black and white figures are suggested to be avoided, however, acceptable.

The figures should be: tiff, jpg or eps files, 300 dpi at least, photos are 600 dpi at least.

BIOGRAPHY

Max. 500 character size professional biography of the author(s).

CHECKING

The editing board checks the articles and informs the authors about suggested modifications. Since the author is responsible for the content of the article, the author is not liable to accept them.

CONTACT

Please send the manuscript in electronic format to the following e-mail address: femgomze@uni-miskolc.hu and epitoanyag@szte.org.hu or by post: Scientific Society of the Silicate Industry, Budapest, Bécsi út 122–124., H-1034, HUNGARY

We kindly ask the authors to give their e-mail address and phone number on behalf of the quick conciliation.

Építőanyag – *Journal of Silicate Based and Composite Materials*, Quarterly peer-reviewed periodical of the Hungarian Scientific Society of the Silicate Industry, SZTE.
http://epitoanyag.org.hu

E-MRS

European Materials Research Society

E-MRS now has more than 4,000 members from industry, government, academia and research laboratories, who meet regularly to debate recent technological developments of functional materials. The E-MRS differs from many single-discipline professional societies by encouraging scientists, engineers and research managers to exchange information on an interdisciplinary platform, and by recognizing professional and technical excellence by promoting awards for achievement from student to senior scientist level. As an adhering body of the International Union of Materials Research Societies (IUMRS), the E-MRS enjoys and benefits from very close relationships with other Materials Research organizations elsewhere in Europe and around the world.

23 RUE DU LOESS, BP 20 - 67037
STRASBOURG CEDEX 02, FRANCE
EMRS@EUROPEAN-MRS.COM
WWW.EUROPEAN-MRS.COM